Article

SOURCE
DATA

TRANSPARENT
PROCESS

EMBO
reports

Characterization of the c10orf76-PI4KB complex and its necessity for Golgi PI4P levels and enterovirus replication

Jacob A McPhail[1] (iD), Heyrhyoung Lyoo[2,†], Joshua G Pemberton[3,†], Reece M Hoffmann[1] (iD), Wendy van Elst[2], Jeroen RPM Strating[2] (iD), Meredith L Jenkins[1], Jordan TB Stariha[1], Cameron J Powell[1], Martin J Boulanger[1], Tamas Balla[3,*] (iD), Frank JM van Kuppeveld[2,**] (iD) & John E Burke[1,***] (iD)

Abstract

The lipid kinase PI4KB, which generates phosphatidylinositol 4-phosphate (PI4P), is a key enzyme in regulating membrane transport and is also hijacked by multiple picornaviruses to mediate viral replication. PI4KB can interact with multiple protein binding partners, which are differentially manipulated by picornaviruses to facilitate replication. The protein c10orf76 is a PI4KB-associated protein that increases PI4P levels at the Golgi and is essential for the viral replication of specific enteroviruses. We used hydrogen–deuterium exchange mass spectrometry to characterize the c10orf76-PI4KB complex and reveal that binding is mediated by the kinase linker of PI4KB, with formation of the heterodimeric complex modulated by PKA-dependent phosphorylation. Complex-disrupting mutations demonstrate that PI4KB is required for membrane recruitment of c10orf76 to the Golgi, and that an intact c10orf76-PI4KB complex is required for the replication of c10orf76-dependent enteroviruses. Intriguingly, c10orf76 also contributed to proper Arf1 activation at the Golgi, providing a putative mechanism for the c10orf76-dependent increase in PI4P levels at the Golgi.

See also: **L Voilquin et al** (February 2020)

Introduction

Phosphoinositides are essential regulatory lipids that play important roles in myriad cellular functions. The phosphoinositide species phosphatidylinositol 4-phosphate (PI4P) is widely distributed and involved in the coordinated regulation of membrane trafficking, cell division, and lipid transport [1,2]. Multiple human pathogens manipulate PI4P levels to mediate their intracellular replication, including *Legionella* [3] and multiple picornaviruses [4,5]. PI4P in humans is generated through the action of four phosphatidylinositol 4-kinases: PI4KIIα (PI4K2A), PI4KIIβ (PI4K2B), PI4KIIIα (PI4KA), and PI4KIIIβ (PI4KB) [6–8]. PI4KB is localized at the Golgi and trans-Golgi network (TGN), with PI4P pools in the Golgi apparatus generated by both PI4K2A and PI4KB [9]. While the localization and activity of PI4K2A is regulated through its palmitoylation, local membrane composition, and cholesterol levels [10], the activity of PI4KB is regulated by multiple protein–protein interactions and phosphorylation [11–14]. These regulatory protein–protein interactions are in turn manipulated by many pathogenic RNA viruses that have evolved the ability to hijack PI4KB and generate PI4P-enriched replication organelles, which are essential for viral replication [15]. For most picornaviruses, manipulation of PI4P levels is driven by the action of the viral 3A protein and its interactions with PI4KB-binding proteins [13,16–18].

PI4KB plays both important catalytic and non-catalytic functions, with its regulation controlled by interactions with multiple protein binding partners, including acyl CoA Binding Domain 3 (ACBD3), Rab11, 14-3-3, and c10orf76 (chromosome 10, open-reading frame 76, also referred to as Armadillo-like helical domain-containing protein 3 (ARMH3)). PI4KB is a multi-domain lipid kinase containing a disordered N-terminus, a helical domain, and a bi-lobal kinase domain

1   Department of Biochemistry and Microbiology, University of Victoria, Victoria, BC, Canada
2   Department of Infectious Diseases & Immunology, Virology Division, Faculty of Veterinary Medicine, Utrecht University, Utrecht, The Netherlands
3   Section on Molecular Signal Transduction, Eunice Kennedy Shriver National Institute of Child Health and Human Development, National Institutes of Health, Bethesda, MD, USA
    *Corresponding author. Tel: +1 301 435 5637; E-mail: ballat@mail.nih.gov
    **Corresponding author. Tel: +31 30 253 4173; E-mail: F.J.M.vanKuppeveld@uu.nl
    ***Corresponding author. Tel: +1 250 721 8732; E-mail: jeburke@uvic.ca
    †These authors contributed equally to this work

[14,19]. Biophysical and biochemical studies have defined the domains of PI4KB that mediate complex formation with protein binding partners. The helical domain of PI4KB forms a non-canonical interaction with the small GTPase Rab11a that mediates localization of a pool of Rab11 to the Golgi and TGN [14,20]. PI4KB is primarily localized to the Golgi through the interaction of its N-terminus with ACBD3 [12,13]. PI4KB is activated downstream of ADP-ribosylation factor 1 (Arf1) [21]; however, no evidence for a direct Arf1-PI4KB interface has been found, suggesting that this may be an indirect effect. PI4KB contains phosphorylation sites in disordered linkers between domains, including Ser294 in the helical-kinase linker of PI4KB, which is phosphorylated by protein kinase D (PKD). Phosphorylation of Ser294 drives binding of 14-3-3, which stabilizes PI4KB, prevents degradation, and increases Golgi PI4P levels [22–24]. Ser496 in the N-lobe linker of PI4KB is phosphorylated by protein kinase A (PKA) [25] and drives PI4KB localization from the Golgi to nuclear speckles [26]. c10orf76 was identified as a putative PI4KB interacting partner in immunoprecipitation experiments [17,27], with knockout of c10orf76 leading to decreased Golgi PI4P levels [28]. The role of this protein is not known; however, it contains a domain of unknown function (DUF1741) that is well conserved in many eukaryotes.

Enterovirus proteins do not interact directly with PI4KB—they instead recruit PI4KB-regulatory proteins. A key component of manipulating PI4KB to generate PI4P-enriched replication organelles is the interaction of viral 3A proteins with host PI4KB-binding proteins. The 3A proteins from enteroviruses (i.e., Poliovirus, Rhinovirus, Coxsackievirus, Rhinovirus, and Enterovirus 71) and Aichivirus recruit PI4KB to replication organelles through an interaction with ACBD3 [11,13,16–18,29–32]. The viral 3A protein from Aichivirus forms a direct interaction with the GOLD domain of ACBD3, leading to redistribution of PI4KB to replication organelles [11,31]. Enteroviruses also manipulate other lipid signaling pathways, with viral 3A proteins able to recruit the protein Golgi-specific brefeldin A-resistance guanine nucleotide exchange factor 1 (GBF1) that activates Arf1 [4,33–35], and subvert Rab11-positive recycling endosomes to replication organelles [36]. A new component of the PI4KB hijacking process, c10orf76, was identified as a key host factor in the replication of coxsackievirus A10 (CVA10) replication, but not coxsackievirus B1 (CVB1) [28].

We hypothesized that a direct c10orf-PI4KB interaction may be critical for the regulation of Golgi PI4P levels and play a role in enterovirus replication. To elucidate the role of c10orf76 in PI4KB-mediated signaling, we utilized a synergy of hydrogen–deuterium exchange mass spectrometry (HDX-MS) and biochemical assays to characterize the novel c10orf76-PI4KB complex *in vitro*. This allowed us to engineer complex-disrupting mutations that were subsequently used to define the role of the c10orf76-PI4KB complex in Golgi PI4P-signaling and viral replication *in vivo*. We find that PI4KB and c10orf76 form a high-affinity complex mediated by a disorder-to-order transition of the kinase linker of PI4KB, with complex affinity modulated by PKA phosphorylation of the c10orf76 binding site on PI4KB. Knockout of c10orf76 leads to decreased PI4P levels and disruption of Arf1 activation in cells. Complex-disrupting mutations revealed that c10orf76 is recruited to the Golgi by PI4KB, and that viral replication of enteroviruses that require c10orf76 is mediated by the c10orf76-PI4KB complex.

Results

c10orf76 forms a direct, high-affinity complex with PI4KB

c10orf76 was previously identified as a putative PI4KB-binding partner through immunoprecipitation experiments [17,27]; however, it was not clear if this was through a direct interaction. To identify a potential direct interaction between PI4KB and c10orf76 *in vitro*, we purified recombinant full-length proteins using a baculovirus and *Spodoptera frugiperda (Sf9)* expression system. Experiments on PI4KB used the slightly smaller isoform 2 variant (1–801, uniprot: Q9UBF8-2), compared to PI4KB isoform 1 (1–816 uniprot: Q9UBF8-1), similar to previous structural studies [14]. His-pulldown assays using NiNTA-agarose beads and purified recombinant proteins showed a direct interaction between PI4KB and His-tagged c10orf76 (Fig 1A). Pulldown experiments carried out with the PI4KB binding partners Rab11 and ACBD3 revealed that although c10orf76 did not directly bind Rab11 or ACBD3 alone, it could form ternary PI4KB-containing complexes with both (Fig EV1), indicating a unique c10orf76 binding interface on PI4KB compared to Rab11 and ACBD3. To examine the stoichiometry of the c10orf76-PI4KB complex, we subjected apo c10orf76 (79 kDa) and c10orf76 with PI4KB (89 kDa) to size-exclusion chromatography. Apo c10orf76 eluted from the size-exclusion column at a volume consistent with a monomer, while the c10orf76-PI4KB complex (158 kDa) eluted at a volume consistent with a 1:1 complex (Fig 1B). Since cellular knockout of c10orf76 has been shown to reduce PI4P levels *in vivo* [28], we investigated the effect of c10orf76 on PI4KB lipid kinase activity with biochemical membrane reconstitution assays using phosphatidylinositol (PI) vesicles. Intriguingly, c10orf76 was a potent inhibitor of PI4KB, with inhibition being dose-dependent and possessing an IC_{50} of ~90 nM (Fig 1C). This inhibitory effect was observed on both pure phosphatidylinositol (PI) vesicles, and vesicles that mimic the composition of the Golgi (20% PI, 10% PS, 45% PE, 25% PC) (Fig 1D). This paradoxical PI4KB-inhibitory result *in vitro* conflicts with observed Golgi PI4P decreases in c10orf76 deficient cells [28]. This suggests that biochemical assays may not fully recapitulate the environment of the Golgi. To further define the role of this complex, we focused on defining the molecular basis of this interface, allowing for generation of binding-deficient mutants for downstream cellular and viral experiments.

HDX-MS reveals that PI4KB and c10orf76 form an extended interface involving a disorder-to-order transition of the PI4KB N-lobe linker

To identify the putative interface between PI4KB and c10orf76, we employed hydrogen–deuterium exchange mass spectrometry (HDX-MS) to map regions protected in both proteins upon complex formation. HDX-MS is an analytical technique that measures the exchange rate of amide hydrogens in proteins. Because one of the main determinants for amide exchange is the presence of secondary structure, their exchange rate is an excellent readout of protein dynamics. HDX-MS is thus a potent tool to determine protein–protein, protein–ligand, and protein–membrane interactions [37–39]. H/D exchange was carried out for three different conditions: apo PI4KB, apo c10orf76, and a 1:1 complex of PI4KB with c10orf76. Deuterium incorporation experiments were carried out at
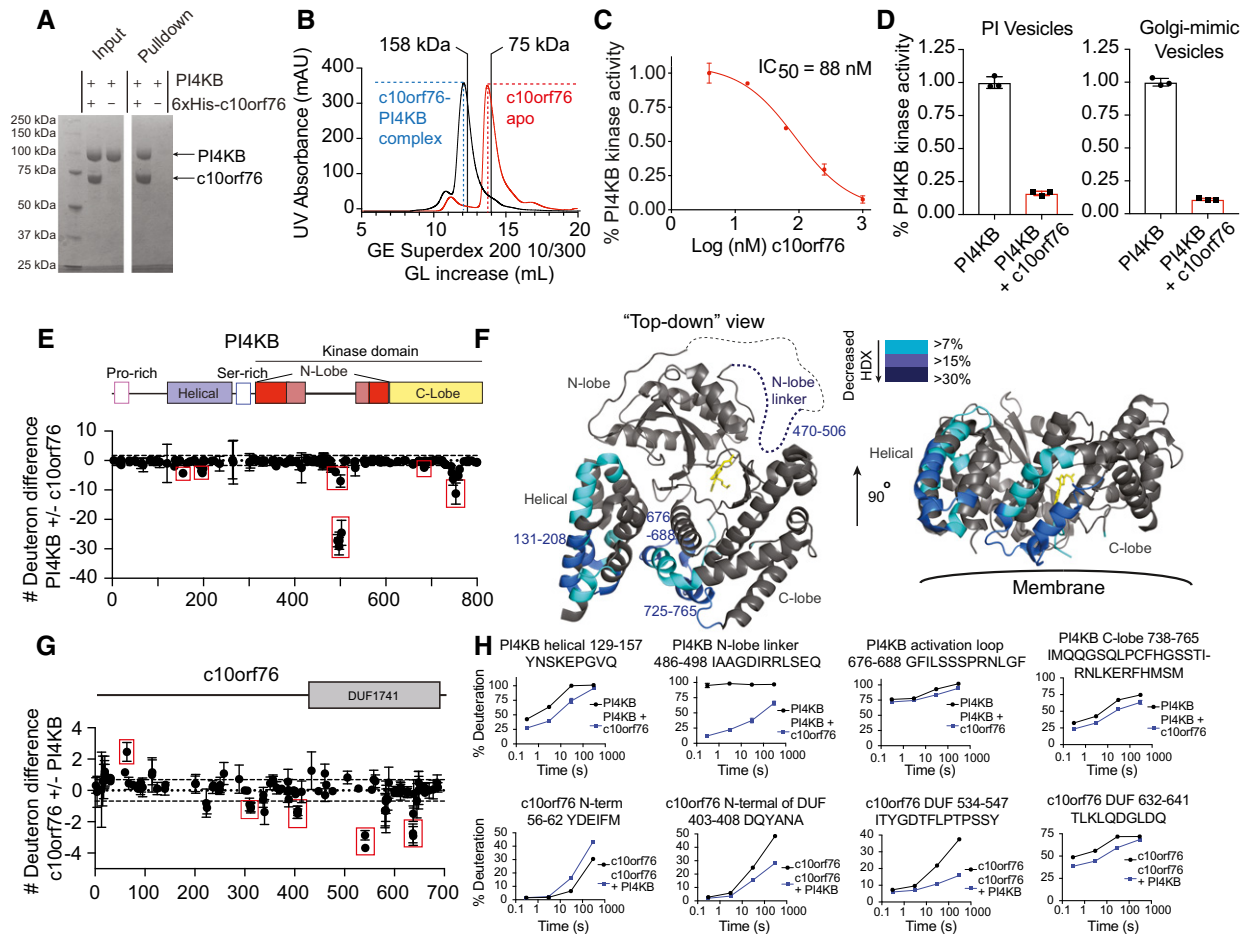
Figure 1. c10orf76 directly binds to PI4KB through an extended interface focused at the N-lobe kinase linker of PI4KB.

A   Recombinant c10orf76 directly binds to PI4KB *in vitro*. His-pulldown assays of baculovirus/*Sf9* produced 6xHis-c10orf76 (3 μM) were carried out with untagged PI4KB (2.5 μM).

B   PI4KB and c10orf76 form a stable complex. The complex of c10orf76-PI4KB eluted from a S200 superdex 10/300 GL increase gel filtration column (GE) at a volume consistent with a heterodimer (169 kDa), while c10orf76 alone eluted at a volume consistent with a monomer (79 kDa). Lines with MW values indicate elution of MW standards (158 kDa aldolase, 75 kDa conalbumin).

C   PI4KB is potently inhibited by c10orf76 in a dose-dependent manner *in vitro*. Kinase assays of PI4KB (20 nM) in the presence of varying concentrations of c10orf76 (1.6 nM–1 μM) were carried out on pure PI lipid vesicles (0.5 mg/l) in the presence of 100 μM ATP. The data were normalized to the kinase activity of PI4KB alone. IC_{50} values were determined by one binding site, nonlinear regression (curve fit) using Graphpad. Error bars represent standard deviation of independent technical replicates ($n = 3$).

D   PI4KB is potently inhibited by c10orf76 on pure PI vesicles and vesicles mimicking Golgi composition. Kinase assays of PI4KB and c10orf76 were carried out on lipid substrate composed of pure PI vesicles (0.5 mg/ml) with 100 μM ATP, and Golgi-mimic vesicles (0.5 mg/ml, 10% PS, 20% PI, 25% PE, 45% PC) with 10 μM ATP. PI4KB was present at 20 and 300 nM in the PI and Golgi substrate assays, respectively, with c10orf76 present at 500 nM in both experiments. The data are normalized to the kinase activity of PI4KB alone. Error bars represent standard deviation of independent technical replicates ($n = 3$).

E   Changes in deuterium incorporation PI4KB in the presence of c10orf76 showed a profound ordering of the kinase domain N-lobe linker and smaller changes in the helical domain and C-lobe of the kinase domain. The sum of the difference mapped as the difference in number of deuterons incorporated for PI4KB (400 nM) in the presence and absence of c10orf76 (400 nM) over all time points (3 s at 1°C; 3 s, 30 s, and 300 s at 23°C). Each dot represents a peptide graphed on the *x*-axis according to the central residue. The red boxes highlight key regions that showed significant changes (> 7% decrease in exchange, > 0.5 Da difference, and unpaired two-tailed student *t*-test $P < 0.05$). Error bars represent standard deviation of independent technical replicates ($n = 3$).

F   c10orf76 binding induces differences in HDX throughout multiple domains of PI4KB. Regions of > 7% difference in deuterium exchange in the presence of c10orf76 are colored onto the structure of PI4KB according to the legend (PDB: 4D0L). The N-lobe linker of the kinase domain is disordered in the structure and is represented by a dotted line.

G   Changes in the deuterium incorporation of c10orf76 in the presence of PI4KB. H/D exchange reactions displayed as the sum of the difference in HDX in the number of deuterons for c10orf76 (400 nM) in the presence of PI4KB (400 nM) at all time points (3 s at 1°C; 3 s, 30 s, and 300 s at 23°C) analyzed. Red boxes highlight regions that showed significant changes (> 7% decrease in exchange, > 0.5 Da difference, and unpaired two-tailed Student's *t*-test $P < 0.05$). Error bars represent standard deviation of independent technical replicates ($n = 3$).

H   The PI4KB N-lobe linker undergoes a disorder-to-order transition upon binding c10orf76. Selected peptides (including the sequence, domain information, and numbering) of both PI4KB and c10orf76 displayed as the % deuteration incorporation over time. Error bars represent standard deviation of independent technical replicates ($n = 3$) and are typically smaller than the size of the point on the graph.

Source data are available online for this figure.

four different timepoints (3, 30, and 300 s at 23°C and 3 s at 1°C). Deuterium incorporation is determined by quenching the exchange reaction in a solution that dramatically decreases the exchange rate, followed by rapid digestion, peptide separation, and mass analysis. A total of 185 peptides covering 96.9% of the PI4KB sequence, and 108 peptides covering 73.9% of the c10orf76 sequence were generated (Fig 1E–H-source data 1, Fig EV2). Significant differences in deuterium exchange between conditions were defined as changes in exchange at any timepoint that met the three following criteria: > 7% change in deuterium incorporation, a > 0.5 Da difference in peptide mass, and a *P*-value of < 0.05 (unpaired Student's *t*-test).

Multiple regions of PI4KB were protected from amide exchange in the presence of c10orf76, revealing an extended binding interface (Figs 1E, F, and H, and EV2). The most prominent difference in exchange was at the C-terminus of the disordered N-lobe linker (residues 486–498), where the presence of c10orf76 led to a significant ordering of this region. This region had no protection from amide exchange in the apo state, revealing it to be disordered, with a very strong stabilization (> 80% decrease in exchange) in the presence of c10orf76, indicating a disorder-to-order transition upon c10orf76 binding (Fig 1H). This N-lobe kinase linker is dispensable for lipid kinase activity, as it can be removed with a minimal effect on PI4KB catalytic activity [19]. In addition to this change, there were multiple smaller decreases in exchange in the helical domain (131–138, 149–157, 159–164, and 183–204) and kinase domain (676–688, 725–734, and 738–765). The helical domain of PI4KB mediates binding to Rab11. However, the PI4KB-Rab11 complex was still able to form in the presence of c10orf76 (Fig EV1). The decreases in exchange with c10orf76 observed in the kinase domain were located in the activation loop (676–688) and the C-lobe (738–765), which may mediate the inhibition observed *in vitro*. The protected surface on PI4KB extensively spans the membrane face of the kinase, which may prevent PI4KB from directly interfacing with

the membrane and accessing PI in the presence of c10orf76, at least in the absence of other binding partners *in vitro* (Fig 1F).

The presence of PI4KB also caused multiple differences in H/D exchange in c10orf76, with increased exchange at the N-terminus (56–62) as well as decreased exchange N-terminal of, and within, the domain of unknown function (DUF1741; 403–408, 534–547, 632–641; Figs 1G and H, and EV2). There are no clear structural determinants of c10orf76, with limited homology to any previously solved structure; however, it is predicted to consist of a primarily helical fold arranged into armadillo repeats. The uncharacterized DUF1741 domain of c10orf76 is present throughout many eukaryotes; however, even though the DUF1741 domain is strongly conserved in evolution, c10orf76 is the only protein that contains this domain in humans.

The largest observed change in deuterium incorporation in either protein was in the PI4KB N-lobe linker (486–496). Interestingly, this region contains a consensus PKA motif (RRxS) that corresponds to Ser496 (Ser511 in PI4KB isoform 1), which is phosphorylated *in vivo* and conserved back to the teleost fishes (Fig 2A) [26]. System-level analysis of PKA signaling networks also shows that phosphorylation of this site is decreased > 90% in PKA knockout cells, indicating that it is likely a direct PKA target [25]. To better understand the regulation of the c10orf76-PI4KB complex, we sought to characterize the effects of Ser496 phosphorylation.

PI4KB is directly phosphorylated at Ser496 by PKA to modulate the affinity of the c10orf76-PI4KB complex

There are three well-validated phosphorylation sites on PI4KB: Ser294, Ser413, Ser496 [40]. To test the role of phosphorylation of PI4KB at Ser496, we generated stoichiometrically phosphorylated PI4KB at only Ser496 using an *in vitro* phosphorylation approach that relied on the production of the purified mouse PKA catalytic subunit in *E. coli*. To minimize complications from any background

Figure 2. The PI4KB c10orf76 interface is conserved and can be post-translationally modified by PKA, with rationally designed mutations disrupting complex formation. ▶

A   The N-lobe kinase linker region of PI4KB is strongly conserved back to *D. rerio*. The N-lobe linker region of PI4KB sequences of the organisms indicated was analyzed using Clustal Omega/ESpript 3. The consensus PKA motif (RRXS) that is conserved back to *D. rerio* is indicated on the sequence, as well as the RL494EA point mutation.

B   The N-lobe kinase linker of PI4KB can be efficiently phosphorylated by PKA. Recombinant PKA at different concentrations (0, 7, 34, 168, or 840 ng) was incubated with recombinant (*E. coli*) wild-type PI4KB (20 μg) for 1 h with 200 μM ATP, and the amount of phosphorylation was followed using mass spectrometry. Relative abundance of Ser496 phosphorylated PI4KB was calculated using the relative intensity (total area) of the phosphorylated vs non-phosphorylated peptide (486–506).

C   PI4KB phosphorylation by PKA alters the affinity for c10orf76. The kinase activity of different variants of PI4KB (15 nM) was measured in the presence of varying amounts of c10orf76 (23 nM–1.5 μM) with 100% PI lipid substrate (0.5 mg/l) and 100 μM ATP. The data were normalized to the kinase activity of PI4KB alone. Error bars represent standard deviation of independent technical replicates (*n* = 3).

D   PI4KB has the same kinase activity when Ser496 is phosphorylated or mutated to alanine. Kinase assay of PI4KB non-phosphorylated, phos-Ser496, or S496A (15 nM) on pure PI lipid vesicles (0.5 mg/l) with 100 μM ATP. The data were normalized to the kinase activity of WT PI4KB. Error bars represent standard deviation of independent technical replicates (*n* = 3).

E   Engineered RL494EA PI4KB mutant shows decreased binding to c10orf76. His-pulldown assays of 6xHis-c10orf76 (3 μM) with wild-type or RL494EA PI4KB (1–2 μM).

F   RL494EA PI4KB activity is not inhibited by c10orf76. Kinase assays of either wild-type or mutant RL494EA PI4KB (40 nM) were carried out with varying concentrations of c10orf76 (3.9 nM–2 μM) with 100% PI lipid vesicles (0.5 mg/l) and 100 μM ATP. The data were normalized to the kinase activity of PI4KB alone. Error bars represent standard deviation of independent technical replicates (*n* = 3).

G   Wild-type PI4KB and RL494EA PI4KB mutant have the same lipid kinase activity. Kinase assays of either wild-type and mutant PI4KB (10 nM) were carried out with 100% PI lipid vesicles (0.5 mg/l), 100 μM ATP, and PI4KB (300 nM) on Golgi-mimic vesicles (0.5 mg/ml) with 10 μM ATP. The data were normalized to the kinase activity of WT PI4KB. Error bars represent standard deviation of independent technical replicates (*n* = 3).

H   FLH409AAA-c10orf76 mutant shows decreased affinity for PI4KB. His-pulldown assays of 6xHis-c10orf76 (1 μM) with wild-type PI4KB (1 μM). Samples washed a total of four times.

I   Kinase assay shows FLH409AAA c10orf76 inhibition of PI4KB is greatly reduced. Kinase assay of PI4KB (40 nM) and a concentration curve of c10orf76 (3.9 nM–2 μM) on pure PI lipid vesicles (0.5 mg/l) with 100 μM ATP. The data were normalized to the kinase activity of PI4KB alone. Error bars represent standard deviation of independent technical replicates (*n* = 3).

J   The PI4KB-binding region of c10orf76 is strongly conserved back to *D. rerio*. Clustal Omega/ESpript 3 alignment of the FLH409 region of c10orf76 that binds PI4KB.
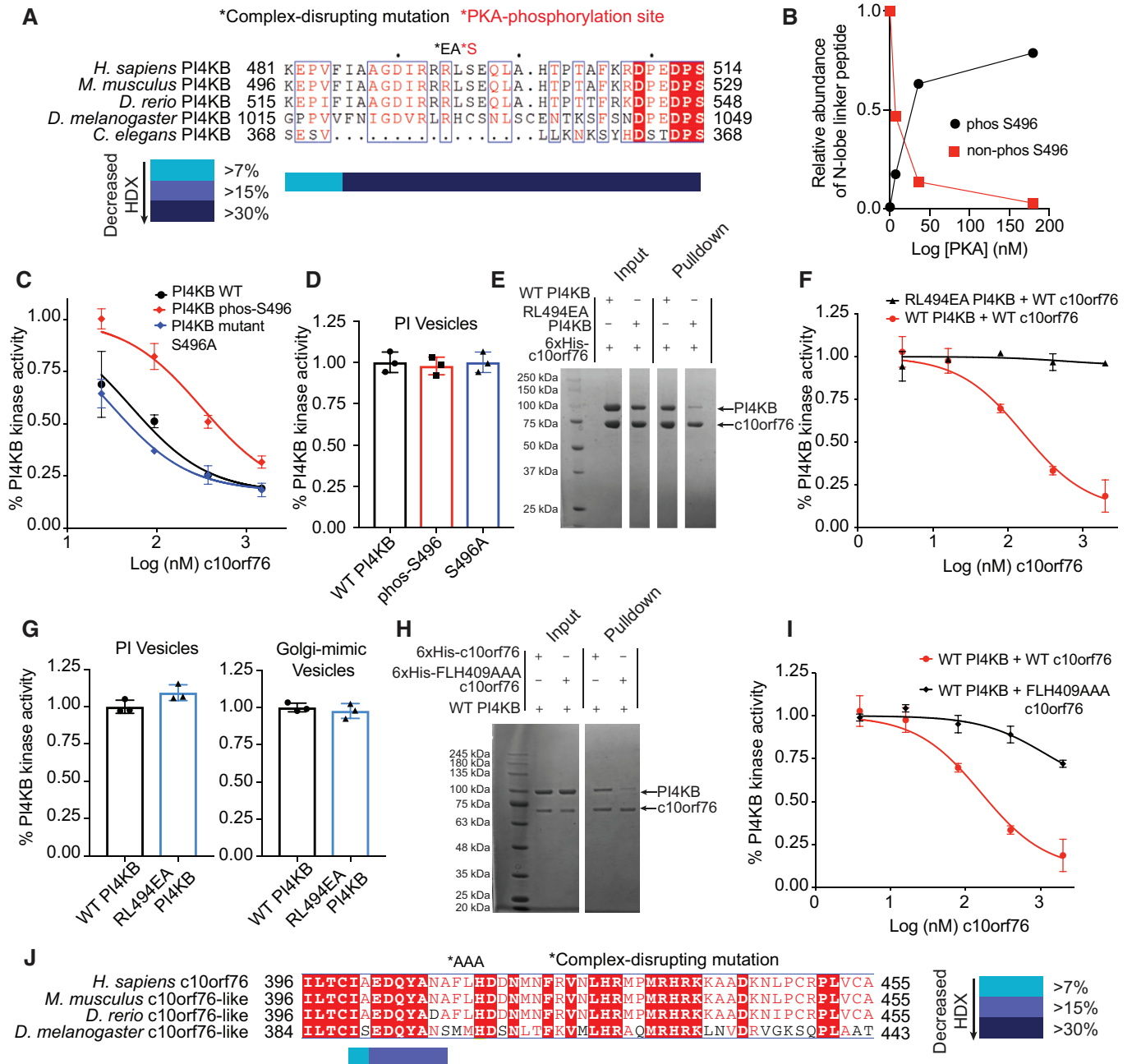
Figure 2.

phosphorylation that occurs in *Sf9* cells, we used PI4KB expressed in *E. coli* to ensure the starting protein substrate was non-phosphorylated. Analysis of the *Sf9*-produced PI4KB revealed significant phosphorylation of Ser294, Ser413, Ser430 and Ser496, while *Sf9*-produced c10orf76 had evidence of phosphorylation of Ser14, and an additional Ser/Thr phosphorylation in the 325–351 region, although the specific residue is ambiguous from the MS data. No phosphorylation was identified from *E. coli*-produced proteins, as expected (Fig EV3). Dose–response assays for the phosphorylation of PI4KB Ser496 using *E. coli*-produced protein were then carried out with increasing concentrations of purified PKA, and the resulting product was analyzed by mass spectrometry to define the site-specific incorporation of phosphate (Fig 2B). Ser496 in PI4KB was

phosphorylated efficiently by PKA, with > 99% phosphorylation at Ser496 occurring with a 1:500 ratio of PKA to PI4KB and no detectable phosphorylation at the other major PI4KB phosphorylation sites (Fig EV3). Lipid kinase assays were then carried out using different concentrations of c10orf76 for both phosphorylated and non-phosphorylated PI4KB. The phosphorylated form had a 3-fold increase in the IC_{50} value, suggesting that Ser496 phosphorylation decreases c10orf76 binding affinity, with no shift in the IC_{50} value for the S496A PI4KB mutant (Fig 2C). Kinase assays carried out on both Ser496 phosphorylated PI4KB and non-phosphorylated PI4KB showed that there is no direct effect of the phosphorylation events on basal lipid kinase activity (Fig 2D). PKA-mediated phosphorylation-dependent changes in the affinity of protein–protein complexes

have been previously described [41,42]. We utilized HDX-MS to test whether the altered inhibition profile we saw was due to decreased affinity between c10orf76 and PI4KB, a method previously utilized to quantify the affinity of protein interactions [43]. These experiments were carried out at a single time point of D_2O exposure (5 s at 20°C) with differing levels of c10orf76 present. Plotting the difference in deuterium incorporation versus c10orf76 concentration gives a characteristic binding isotherm for both phosphorylated and non-phosphorylated PI4KB; displaying a 2- to 3-fold decreased affinity for the phosphorylated form of PI4KB (85 nM vs. 36 nM, Fig EV3). Phosphorylated PI4KB Ser496 also displayed a ~2-fold decrease in affinity for c10orf76 when determined by isothermal titration calorimetry (Fig EV3). Phosphomimic PI4KB mutants S496D and S496E did not mimic the phosphorylation-dependent reduction of c10orf76 affinity, so they could not be utilized to study this effect *in vivo* (Fig EV3). To better characterize the role of the c10orf76-PI4KB complex *in vivo*, we sought to generate c10orf76-PI4KB complex-disrupting mutations.

Rationally engineered PI4KB and c10orf76 mutants that disrupt complex formation

The c10orf76 binding site within the N-lobe kinase linker of PI4KB identified by HDX-MS is highly conserved in vertebrates, with much of the region also conserved in *D. melanogaster,* but not in *C. elegans* (Fig 2A). We used a combination of both the sequence conservation and HDX-MS results to design a complex-disrupting mutant. The RL residues at 494–495 were mutated to EA (RL494EA), effectively causing both a charge reversal and decrease in hydrophobicity. The RL494EA mutant disrupted binding to His-tagged c10orf76 bait in a His-pulldown assay (Fig 2E) and prevented inhibition by c10orf76 in kinase assays (Fig 2F). This mutant had exactly the same basal kinase activity as the WT PI4KB on both PI vesicles and Golgi-mimetic vesicles (Fig 2G), strongly suggesting that the mutant kinase is properly folded. In an attempt to design rational mutations of c10orf76 that also disrupted binding to PI4KB, multiple mutations were tested in regions 403–408, 534–547, and 632–641 that were identified using HDX-MS. Combining the HDX-MS data and sequence homology, we designed a triple alanine mutant at the end of a putative helix (QYANAFL, residues 404–410) that was well conserved in vertebrates (Fig 2J), close to the HDX-MS protection (FLH residues 409–411 to AAA, referred to as FLH mutant afterward). The FLH mutant expressed well, significantly reduced binding to PI4KB in a

His-pulldown assay (Fig 2H), and also showed a marked reduction in its ability to inhibit PI4KB activity (Fig 2I). To confirm the c10orf76 FLH mutant does not affect global protein structure, we compared deuterium incorporation of the c10orf76 wild-type and FLH mutant and observed no changes in deuterium incorporation outside of the predicted helix containing the FLH residues (Fig EV4). The engineering of complex-disrupting mutants that do not alter catalytic activity or protein folding provided an excellent tool to test the importance of the c10orf76-PI4KB complex in cells.

PI4KB recruits c10orf76 to the Golgi

To define the role of the c10orf76-PI4KB interface in cellular localization, we utilized fluorescently tagged variants of the wild-type and complex-disrupting mutants of both PI4KB and c10orf76. Fluorescence microscopy of HEK293 cells expressing GFP-tagged wild-type PI4KB revealed that it primarily localizes to the Golgi (Fig 3A). GFP-PI4KB RL494EA, which is deficient in c10orf76 binding, also localized mainly to the Golgi, which suggests that c10orf76 plays a minimal role in the Golgi recruitment of PI4KB (Fig 3A). The wild-type GFP-c10orf76 also localizes to the Golgi. However, the PI4KB binding-deficient FLH mutant is redistributed to the cytosol; revealing an important role for PI4KB in the proper cellular localization of c10orf76 (Fig 3B). Note that the Golgi localization of GFP-PI4KB or GFP-c10orf76 is only visible with low expression levels as the endogenous binding sites are quickly saturated and the excess cytoplasmic GFP-tagged protein eventually masks the Golgi-bound pools at higher levels of expression. To further analyze the role of PI4KB in the recruitment of c10orf76, we utilized a chemically inducible protein heterodimerization system that relies on the selective interaction of the FKBP12 (FK506 binding protein 12) and FRB (a 9 kDa fragment of mTOR that binds rapamycin) modules upon treatment with rapamycin [12,44]. Specifically, we fused the FRB domain to residues 34–63 of a CFP-tagged mitochondrial localization signal from mitochondrial A-kinase anchor protein 1 (AKAP1), and fused mRFP-FKBP12 onto the wild-type or mutant variants of human PI4KB (Fig 3C). These constructs allowed us to examine the localization of the wild-type or mutant GFP-c10orf76 following the acute sequestration of PI4KB to the outer mitochondrial membrane, where other Golgi-associating proteins are not be present. To best demonstrate their co-recruitment upon rapamycin addition, mRFP-FKBP12-PI4KB and eGFP-c10orf76 were expressed at high levels, and thus present as mainly cytosolic due to saturation of endogenous binding

Figure 3. PI4KB recruits c10orf76 to the Golgi *in vivo*.

A   Transfections of HEK293 cells revealed that both wild-type GFP-PI4KB and RL494EA GFP-PI4KB localize to the Golgi.

B   WT c10orf76 also localized to the Golgi; however, the PI4KB binding-deficient mutant of c10orf76 (FLH409AAA) predominantly localized to the cytosol.

C   Cartoon schematic of rapamycin-inducible mitochondria recruitment. The AKAP1-FRB-CFP construct is localized to the outer mitochondrial membrane, while the mRFP-FKBP12-PI4KB and eGFP-c10orf76 are localized in the Golgi as well as within the cytoplasm where they can form a complex. Upon addition of rapamycin, the mRFP-FKBP12-PI4KB construct is translocated to the mitochondria.

D   Mitochondria recruitment experiment with wild-type PI4KB and c10orf76. Left: AKAP1-FRB-CFP is localized to the mitochondria before (top) and 5 min after rapamycin (100 nM) treatment (bottom). Middle: mRFP-FKBP12-PI4KB at high expression level is located in the cytosol before rapamycin (top) and translocates to the mitochondria after rapamycin induction (bottom). Right: eGFP-c10orf76 at a high expression level is located in the cytosol before rapamycin (top) and translocates to the mitochondria after rapamycin induction (bottom).

E   Schematic of the rapamycin-inducible mitochondria recruitment experiment with mutant PI4KB and WT c10orf76.

F   Mitochondria recruitment experiment with mutant PI4KB and WT c10orf76. Left: AKAP1-FRB-CFP is localized to the mitochondria before (top) and 5 min after (bottom) rapamycin treatment. Middle: mRFP-FKBP12-PI4KB(RL494EA) is located in the cytosol before rapamycin (top) and translocates to the mitochondria after rapamycin induction (bottom). Right: eGFP-c10orf76 is located in the cytosol before rapamycin (top) and after (bottom) rapamycin induction.

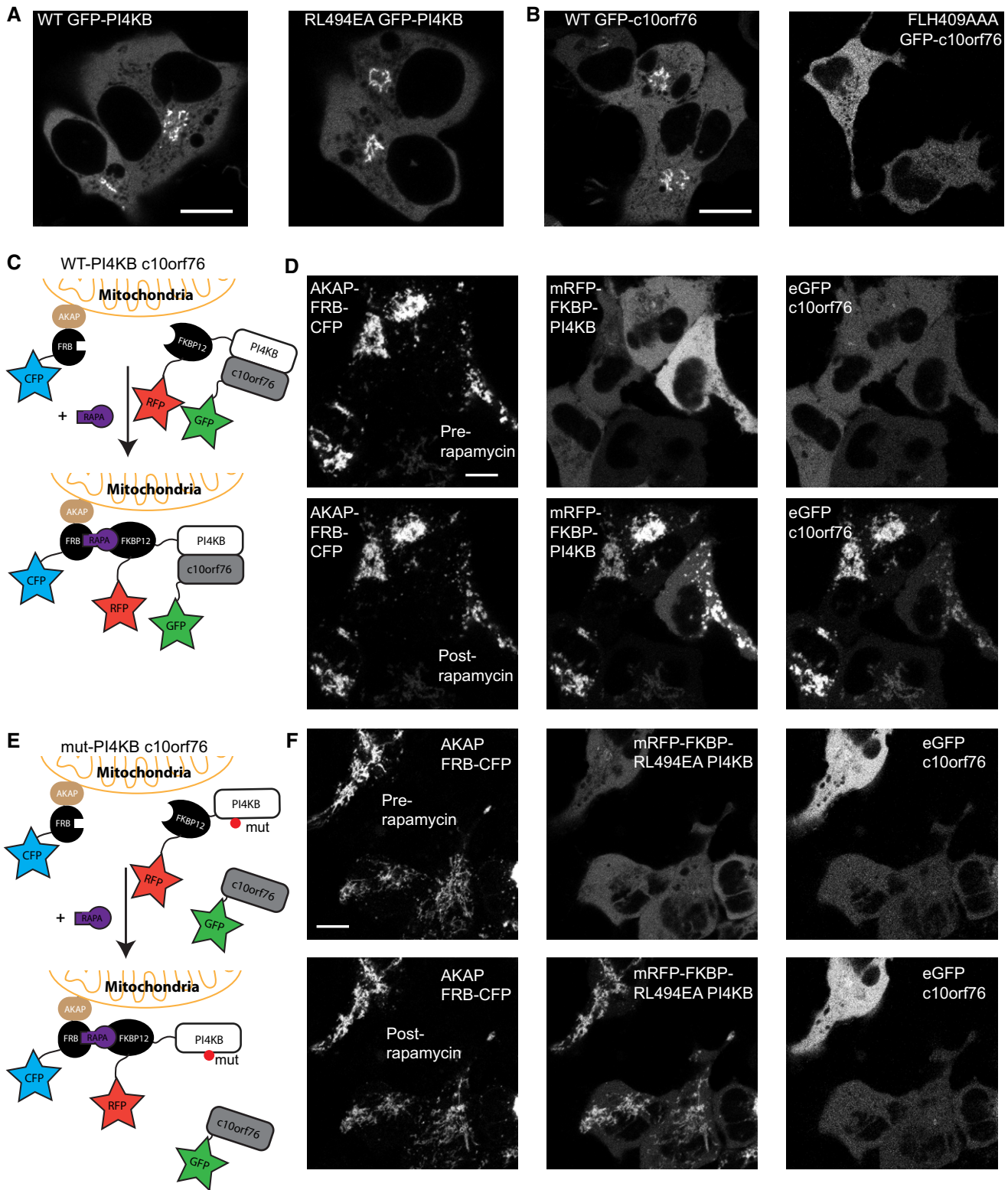Data information: Scale bars represent 10 μm.

Figure 3.

sites (Fig 3D; Movie EV1). Treatment with rapamycin (100 nM) caused the rapid recruitment of mRFP-FKBP12-PI4KB to the mitochondria, which also caused the rapid co-recruitment of c10orf76 (Fig 3D; Movie EV1), suggesting that PI4KB is the only component necessary for membrane recruitment of c10orf76. Experiments using mRFP-FKBP12 PI4KB RL494EA showed that although the mutant kinase is relocated to the mitochondria, GFP-c10orf76 does not co-localize (Fig 3E and F, Movie EV2). To test any effect of the PI4KB

S496 phosphorylation site on localization, although the S496E and S496D mutants did not properly mimic phosphorylation (Fig EV3), recruitment experiments were performed with the non-phosphorylatable PI4KB mutant (S496A). At lower expression levels, mRFP-FKBP12 PI4KB S496A and eGFP-c10orf76 maintained normal Golgi localization, and treatment with rapamycin caused recruitment to the mitochondria (Fig EV5). At higher expression levels, mRFP-FKBP12 PI4KB S496A and eGFP-c10orf76 quickly saturate Golgi sites and flood the cytosol, and treatment with rapamycin caused robust recruitment to the mitochondria, suggesting phosphorylation of PI4KB S496 is not important in the normal localization of either protein (Fig EV5). Taken together, these live-cell studies corroborated the protein interaction studies completed *in vitro* and also demonstrate that the newly defined c10orf76-PI4KB interface is required for proper localization of c10orf76 to the Golgi. Compellingly, these findings reveal a novel function of PI4KB in the recruitment of c10orf76.

c10orf76 regulates active Arf1 dynamics and maintains Golgi PI4P levels

The paradoxical finding that the loss of c10orf76 leads to decreased PI4P levels in cells, yet c10orf76 decreased the catalytic activity of PI4KB *in vitro*, suggested that there was an unknown lipid or protein constituent in cells that is not present in our *in vitro* experiments. To determine the role of c10orf76 in cells, we examined the distribution of different Golgi-localized signaling components in c10orf76-deficient (knockout) HAP1 cells. In agreement with previous studies [28], we found that there were decreased PI4P levels at the Golgi in c10orf76 knockout cells, as indicated by decreased Golgi staining by an anti-PI4P antibody (Fig 4A). Intriguingly, there was an apparent increase in Golgi-localized PI4KB in the c10orf76 knockout cells (Fig 4A), similar to what occurs upon treatment with a PI4KB inhibitor [45], clearly indicating that decreased PI4P production was not due to loss of PI4KB recruitment in the absence of c10orf76. We tested the localization of different Golgi markers to verify that decreased PI4P was not due to disruption of Golgi morphology. Giantin, a marker of the cis/medial Golgi, and ACBD3, which binds to Giantin and recruits PI4KB to Golgi membranes [12,13], both showed similar localization in both WT and c10orf76 knockout cells (Fig 4B). Markers for the cis Golgi (GM130), the trans-Golgi network (TGN46), and the ER–Golgi intermediate compartment (ERGIC53) were also similar, suggesting that Golgi morphology was maintained in the c10orf76 knockout HAP1 cells (Fig 4B).

We next tested the localization of the Arf1-GEF GBF1, as active GTP-bound Arf1 is a putative activator of PI4KB [21]. We confirmed similar expression levels of PI4KB, GBF1, and β-Actin in WT and c10orf76 KO cells to verify any observed differences were not due to protein expression levels (Fig 4C). In c10orf76 knockout cells, there

was a redistribution of GBF1, with GBF1 being more diffuse, with less localized at the Golgi (Fig 4D). The generation of active GTP-bound Arf1 by Arf-GEFs leads to recruitment of multiple effector proteins, with one of most well characterized being the coatomer proteins, which form COPI-coated vesicles that mediate Golgi to ER trafficking. In c10orf76 knockout cells, there was more diffuse staining outside of the Golgi for the active Arf1-binding coatomer components COP-β or COP-α/γ (Fig 4D). Antibody staining with the CM1 antibody, which recognizes the native form of coatomer [46], showed similar distribution for both WT and c10orf76 knockout cells, indicating the formation and distribution of native cytosolic coatomer was not affected (Fig 4D). This puzzling difference may be caused by an altered recruitment of a subset of coatomer components (COP-β or COP-α/γ), and minor effects on the native coatomer complex. Importantly, the major phenotypic observations in the HAP1 c10orf76 knockout cells (i.e., reduced PI4P and increased PI4KB levels on an intact Golgi, and a more diffuse GBF1 and COPI staining with less localization at the Golgi) were also observed in HeLa cells in which c10orf76 was knocked out (H.R. Lyoo and F.J.M. van Kuppeveld, personal observation). Overall, these results suggest that c10orf76 plays a role in the regulation of GBF1/Arf1 dynamics at the Golgi.

Replication of c10orf76-dependent enteroviruses requires intact c10orf76-PI4KB interaction

All enteroviruses depend on PI4KB kinase activity for replication. Despite the physical and functional connection between PI4KB and c10orf76, enteroviruses showed different dependencies on c10orf76 [28]. Specifically, while Coxsackievirus A10 (CVA10) replication was impaired in c10orf76 knockout cells, the replication of CVB1 was not. Furthermore, c10orf76 was identified as a pro-viral factor for replication of poliovirus (PV1) [47]. We set out to investigate the importance of the c10orf76-PI4KB interaction for replication of CVA10 and PV1. We first made a side-by-side comparison of virus replication in HAP1 wild-type and c10orf76 knockout cells in a single cycle of replication. The replication of CVA10 was significantly impaired in c10orf76-deficient cells, with partial inhibition of PV1 replication, and no impairment for replication of CVB3 (Fig 5A). Due to the notoriously difficult nature of transfecting HAP1 cells, we determined the importance of the c10orf76-PI4KB interaction for virus replication in HeLa PI4KB knockout cells transfected with different PI4KB expression plasmids as previously described [29]. Expression of wild-type PI4KB efficiently restored the replication of all viruses (Fig 5B). Expression of the PI4KB RL494EA mutant that is deficient in binding c10orf76 fully rescued replication in CVB3, only partially rescued PV1 replication, and failed to rescue CVA10 replication. These observations suggest that the c10orf76-PI4KB interaction is necessary for CVA10, and to a


Figure 4. **Knockout of c10orf76 in HAP1 cells leads to decreased PI4P levels and disruption of GBF1/active Arf1 localization despite minimal effects on Golgi morphology.**

A, B   HAP1 cells were fixed and stained with antibodies examining PI4P and PI4KB (A) and Golgi morphology markers (B).

C   Western blot of GBF1, PI4KB, and B-Actin levels in both wild-type and c10orf76 KO HAP1 cells.

D   Markers of Arf1 activation—the coatomer proteins COPIα/γ and βCOP act as a readout for GTP-bound Arf1, while the native coatomer was detected with the CM1 antibody.
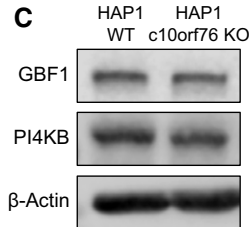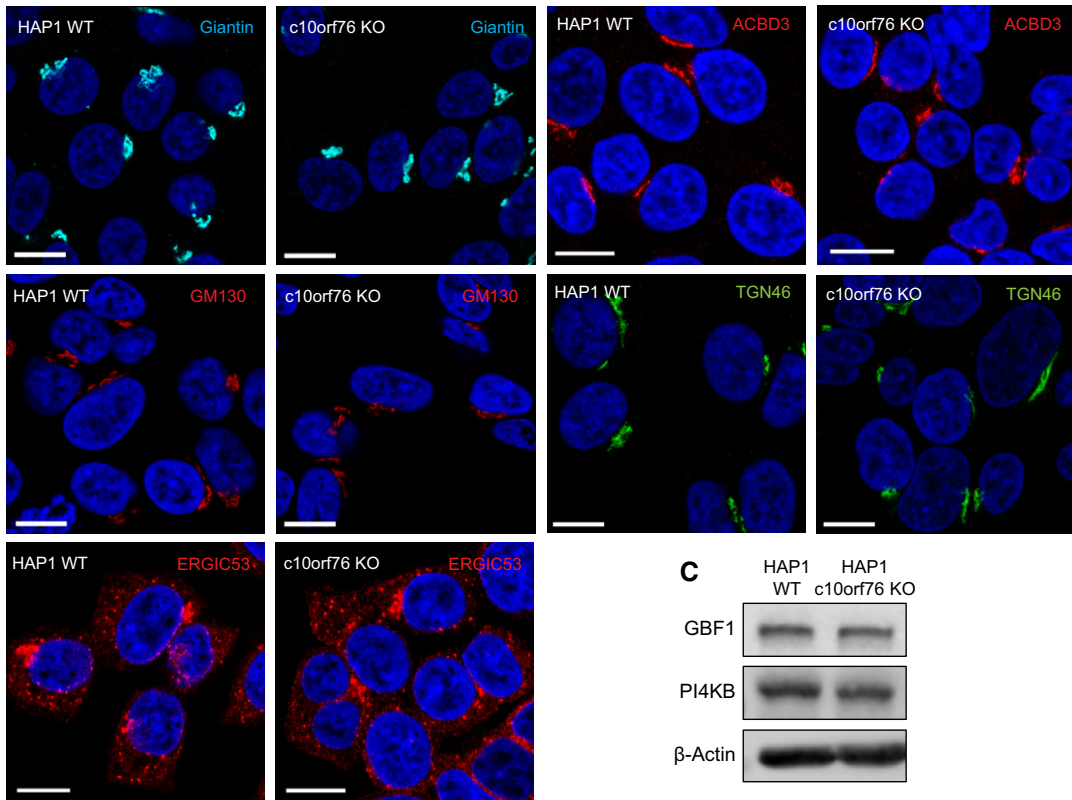
Data information: Nuclei were stained with DAPI (blue). Scale bars represent 10 μm.

A Localization of PI4P and PI4KB in WT and c10orf76 KO HAP1 cells
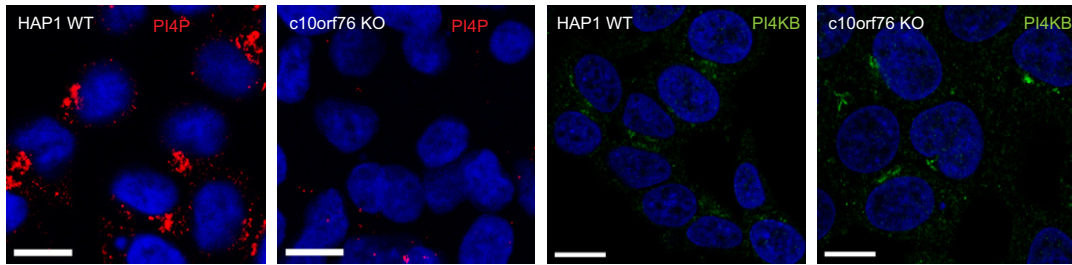
B Localization of Golgi/TGN/ER markers in WT and c10orf76 KO HAP1 cells

C

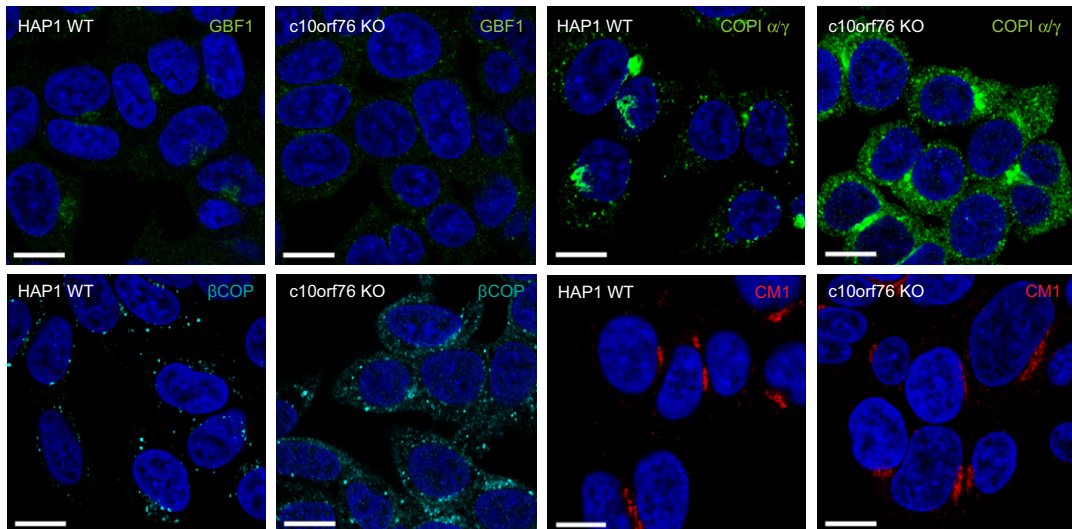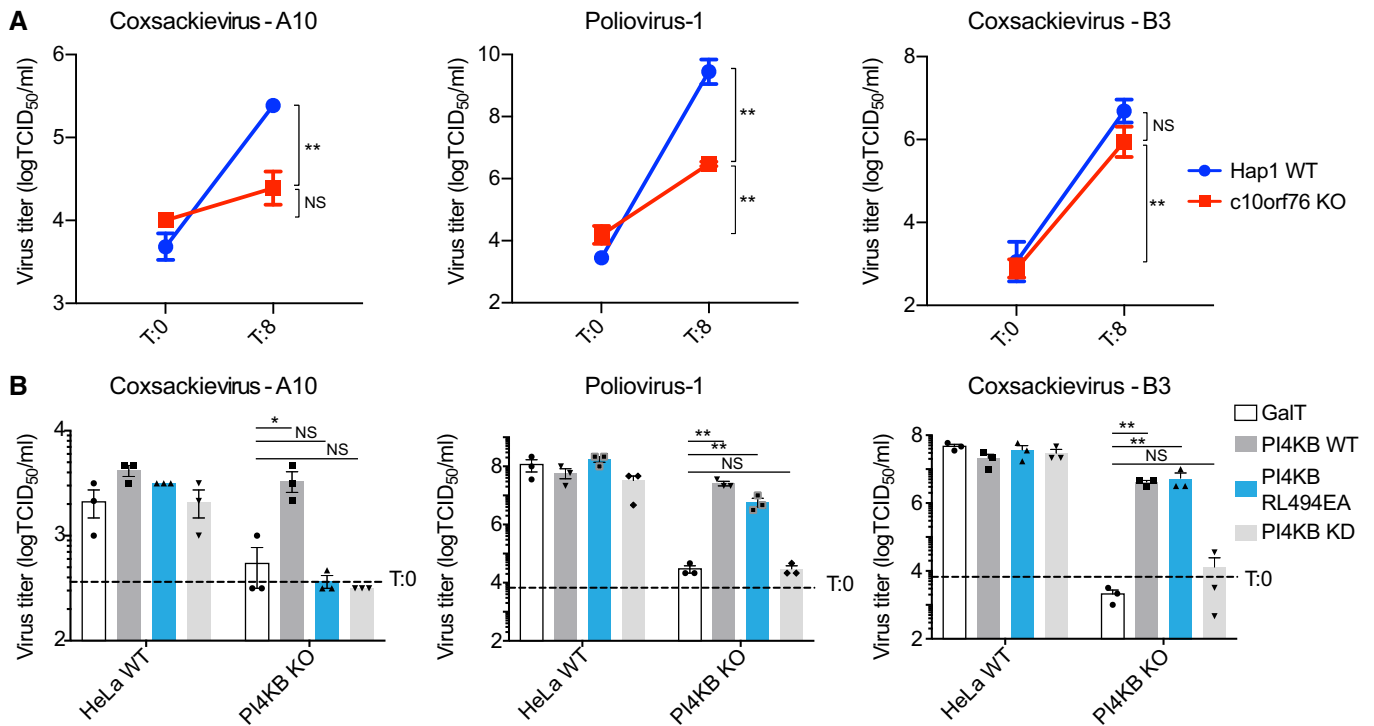D Localization of Arf1 GEFs and effectors in WT and c10orf76 KO HAP1 cells

Figure 4.

Figure 5. The c10orf76-PI4KB complex is essential for Coxsackievirus A10 replication.

A   Viral infection assays determining viral titers by end-point titration at 0 and 8 h in HAP1 wild-type or c10orf76 knockout cells. Left: Coxsackievirus A10 infection. Middle: Poliovirus-1 infection. Right: Coxsackievirus B3 infection. Titer values for c10orf76 knockout cells at 8 h were statistically evaluated compared to c10orf76 knockout titers at 0 h and wild-type titers at 8 h using a one-way ANOVA. **$P < 0.01$; N.S.: $P > 0.05$.

B   Viral infection assays determining virus titers by end-point titration at 8 h in HeLa wild-type and PI4KB knockout cells upon transfection of wild-type PI4KB, the complex-disrupting RL494EA PI4KB mutant or the kinase-dead D674A PI4KB mutant. Left: Coxsackievirus A10 infection. Middle: Poliovirus-1 infection. Right: Coxsackievirus B3 infection. Values were statistically evaluated compared to the GalT control using a one-way ANOVA. **$P < 0.01$; *$P < 0.05$; N.S.: $P > 0.05$.

Data information: For all panels, error bars represent standard error of biological replicates ($n = 3$).

lesser extent, PV1 replication and thereby implies that functions of c10orf76 are selectively hijacked by specific viruses.

Discussion

Defining the full complement of cellular roles for PI4KB is an important objective in characterizing the integrated control of secretion and membrane trafficking at the Golgi, and also provides a framework for understanding how PI4P can be manipulated by viruses. We have identified the c10orf76-PI4KB interaction as an important Golgi signaling complex and a critical factor in the replication of specific enteroviruses. Multiple mechanisms have been previously described for how PI4KB participates in Golgi signaling and membrane trafficking, including detailed insights into protein binding partners, post-translational modifications, and regulated recruitment to specific membrane compartments. PI4KB was originally identified in yeast (yeast protein PIK1) as an essential gene [48], with its activity playing a key role in secretion from the Golgi [49]. The mammalian isoform was identified soon afterward through its sensitivity to wortmannin [50–52]. The first identified Golgi activator of PI4KB was the GTPase Arf1 [21]. However, no direct interaction has been established, which indicates a potential indirect mechanism of activation. Phosphorylation of PI4KB by PKD at

Ser294 mediates binding to 14-3-3 proteins, with this leading to an increase in PI4KB activity [22,23], that has been suggested to correspond with an increase in PI4KB stability [24]. The most well-validated protein binding partner that regulates Golgi recruitment of PI4KB is ACBD3 (previously referred to as GCP60) [13]. ACBD3 forms a direct, high-affinity interface with PI4KB that is mediated by a disorder-to-order transition in the N-terminus of PI4KB upon binding to the Q domain of ACBD3 [11,12]. The recruitment of PI4KB to the Golgi by ACBD3 is controlled through the direct interaction of the GOLD domain of ACBD3 with the Golgi resident transmembrane protein Giantin [53]. In addition to regulatory protein interactions, PI4KB is predicted to contain an amphipathic lipid packing sensor (ALPS) motif at the C-terminus that mediates lipid binding to unsaturated membranes [9]. PI4KB plays key non-catalytic roles through its interaction with the GTPase Rab11, with PI4KB required for localizing a pool of Rab11 to the Golgi and TGN [54]. This interaction is mediated through a non-canonical, nucleotide-independent binding interface with the helical domain of PI4KB [14]. However, there are still many unexplained aspects of PI4KB recruitment and regulation, highlighted by the increased recruitment of PI4KB to the Golgi following treatment with PI4KB inhibitors that is concomitant with a decrease in Golgi PI4P levels [45].

The protein c10orf76 was originally identified as a putative PI4KB interacting partner through co-immunoprecipitation experiments
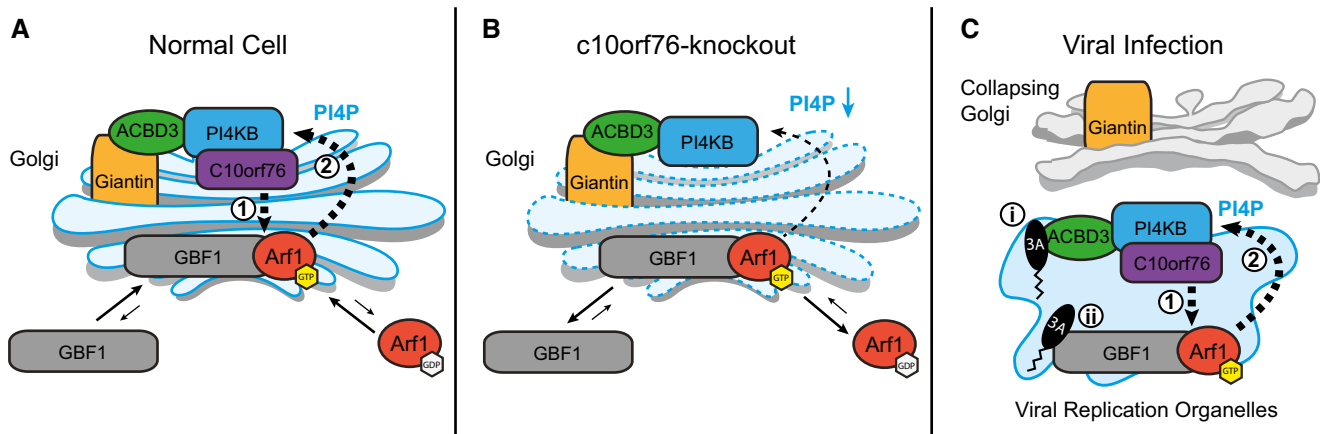
Figure 6. Summary of novel role of c10orf76 in modulating PI4P levels, active Arf1-GTP dynamics, and viral replication.

A At the Golgi, the recruitment of PI4KB can be controlled through the action of ACBD3. PI4KB can recruit c10orf76 to the Golgi, with this playing a role in the dynamics and localization of GBF1 and active Arf1-GTP and their downstream effectors (1). Active, membrane localized Arf1-GTP can activate PI4KB (2).
B In a c10orf76-knockout cell, there is decreased recruitment of GBF1 and active Arf1, with this potentially describing the decreased levels of PI4P.
C In enterovirus infected cells, there are multiple mechanisms that can alter PI4P levels and Arf1 activation. The 3A proteins from different viruses can activate PI4KB, primarily through hijacking ACBD3 (i), as well as directly binding to GBF1 (ii). Viruses that require c10orf76 to replicate rely on the PI4KB-c10orf76 interface, emphasizing the importance of manipulating PI4KB-c10orf76 and GBF1/Arf1-GTP dynamics to facilitate viral replication.

using tagged PI4KB [17,27]. Tests of genetic essentiality identified c10orf76 as a central molecular hub at the Golgi, with it being synthetically lethal in combination with the loss of several different Golgi signaling proteins, and also showing a genetic link to PI4KB [28]. That study also found that c10orf76 is essential in the KBM7 CML cell line, but not in HAP1 cells, with this relationship also being true for PI4KB. Additional evidence on the essentiality of this protein is highlighted by the homozygous mutant of ARMH3, the mouse homolog of c10orf76, which is lethal at the pre-weaning stage [55]. c10orf76 is highly conserved in vertebrates and we find a strong correlation between the conservation of the kinase linker region of PI4KB and the PI4KB-binding site in c10orf76, suggesting that a key role of c10orf76 is linked to its ability to form a complex with PI4KB. PI4KB recruitment to the Golgi is not mediated by c10orf76, but instead it appears that PI4KB is responsible for the Golgi recruitment of c10orf76. *In vitro,* c10orf76 led to decreased lipid kinase activity of PI4KB. However, knockout of c10orf76 in cells led to reduced PI4P levels. This discrepancy could be due to the lack of other PI4KB regulators *in vitro*, such as Arf1/GBF1 or ACBD3, as well as the potential for c10orf76 to alter phosphatidylinositol dynamics. Knockout of c10orf76 led to an increased cytosolic fraction of the Arf GEF GBF1 and active Arf1 effectors (COP-β or COP-α/γ), but not native coatomer, suggesting altered Arf1/GBF1 dynamics in the c10orf76 knockout may be responsible for the disruption of Golgi PI4P levels [21]. This alteration was not due to Golgi disassembly, and despite perturbed Arf1 dynamics the presence of ACBD3 appeared to be sufficient for PI4KB recruitment to Golgi membranes as previously shown [12,13]. The activity of PI4KB is also regulated through the action of phosphatidylinositol transfer proteins (PITPs), which activate PI4KB activity, and c10orf76 may play a role in altering PI dynamics [56]. It is also possible that while PI4KB drives c10orf76 recruitment to the Golgi, endogenous c10orf76 levels *in vivo* engage only a minor fraction of PI4KB, or that c10orf76 itself interacts with other Golgi factors that induce a non-inhibitory confirmation with PI4KB. While further studies will be needed to fully describe the role

of the PI4KB/c10orf76 complex, our work reveals c10orf76 as a novel player in regulation of Arf1 dynamics and corresponding Golgi PI4P levels (Fig 6A and B).

Enteroviruses hijack numerous lipid signaling processes within infected cells to mediate their replication through the generation of replication organelles, with recruitment of PI4KB [4] and GBF1 [33] playing key roles in this process. Recruitment of these cellular host factors in enteroviruses is primarily mediated through the action of membrane-bound viral 3A proteins, which form either direct or indirect interactions that are important for facilitating replication organelle formation. One of the most well-conserved 3A binding partners in enteroviruses is the Golgi resident protein ACBD3, which interacts with the central part of 3A and recruits as well as activates PI4KB [11,13,18,29,31]. The N-terminal part of the 3A proteins from several enteroviruses (*e.g.,* poliovirus and coxsackie virus B3) directly binds and recruits GBF1, but this interaction is less conserved, severely reduced, or even absent in the 3A proteins of rhinoviruses due to subtle amino acid differences in their N-terminus [18,33]. Recently, it has been found that there are multiple mechanisms of recruitment of GBF1 downstream of Poliovirus [57], with c10orf76 potentially being involved in this role. We find that c10orf76 is required for replication of coxsackie virus A10, and to a lesser extent poliovirus, and that c10orf76-dependent viruses rely on the c10orf76-PI4KB interface. Poliovirus is the causative agent of poliomyelitis, and coxsackie virus A10 is an important cause of outbreaks of hand-foot-and-mouth disease, but which is also associated with severe, and sometime fatal, clinical symptoms such as aseptic meningitis. Remarkably, replication of coxsackie virus B1 [28] and coxsackie virus B3 (this study) is independent of c10orf76. Why the c10orf76-PI4KB interface is necessary for replication of some enteroviruses, but not others, is unknown. The differential dependence on c10orf76 could possibly be explained by distinct affinity of 3A proteins from different viruses toward GBF1. Alternatively, each virus may require specific threshold PI4P level for efficient formation of its replication complexes or replication organelles. Together, viral 3A, ACBD3,

GBF1, and c10orf76 play a role in viral replication organelle formation (Fig 6C), although more research on the dependence of viral replication on either GBF1 or c10orf76-mediated alteration of PI4P levels is required to better understand how enteroviruses hijack these complex membrane trafficking processes.

Direct inhibition of PI4KB is likely not a useful antiviral strategy due to unexpected deleterious side effects of PI4KB inhibition in animal models [58]. The targeting of other cellular host factors used to manipulate PI4KB signaling or feedback is a potential avenue for development of novel antiviral therapeutics. Identification of a direct high-affinity c10orf76-PI4KB complex that regulates the cellular localization of c10orf76 represents key insight into the multifaceted regulation of PI4KB signaling. The important role of the c10orf76-PI4KB complex in the replication of select enteroviruses represents a novel molecular platform, which is targeted by viruses that hijack lipid signaling. The involvement of c10orf76 in Arf1 dynamics, as well as the dependence on PI4KB for Golgi localization of c10orf76, reveals a potential role of the c10orf76-PI4KB complex in Arf1 activation and subsequent PI4P production.

Materials and Methods

Protein expression and purification

c10orf76 and PI4KB

The human *C10orf76* gene (Uniprot Q5T2E6) was synthesized by GeneArt (Thermo Fisher). c10orf76 and PI4KB (Uniprot Q9UBF8-2) were each expressed with an N-terminal 6xHis-tag followed by a TEV protease site. The c10orf76 and PI4KB proteins purified for HDX-MS were expressed in *Spodoptera frugiperda* (*Sf9*) cells by infecting 1–4 l of cells at a density of 1.5×10^6 cells/ml with baculovirus encoding the kinase. After 60–72 h infection at 27°C, *Sf9* cells were harvested and washed in phosphate-buffered saline (PBS). The c10orf76 and PI4KB proteins utilized for assays, mutational analysis, and studying PKA phosphorylation were expressed in Rosetta (DE3) *E. coli* (c10orf76) or BL21 C-41(DE3) *E. coli* (PI4KB) induced overnight at 16°C with 0.1 mM IPTG at an OD_{600} of 0.6. Cell pellets containing c10orf76 or PI4KB were sonicated in NiNTA Buffer (20 mM Tris–HCl pH 8.0, 100 mM NaCl, 20 mM imidazole, 5% (v/v) glycerol, 2 mM β-mercaptoethanol) containing protease inhibitors (Millipore Protease Inhibitor Cocktail Set III, Animal-Free) for 5 min on ice. Triton X-100 (0.1% v/v) was added to the cell lysate, and the lysed cell solution was centrifuged for 45 min at 20,000 *g* at 2°C. Supernatant was filtered through a 5 μm filter and loaded onto a 5 ml HisTrap™ FF crude (GE) column in NiNTA buffer. The column was washed with 1.0 M NaCl and 20 mM imidazole in NiNTA buffer, and protein was eluted with 200–250 mM imidazole in NiNTA buffer. Eluted c10orf76 or PI4KB was pooled and concentrated onto a 5 ml HiTrap™ Q column (GE) equilibrated with Q buffer (20 mM Tris–HCl pH 8.0, 100 mM NaCl, 5% glycerol v/v, 2 mM β-mercaptoethanol) and eluted with an increasing concentration of NaCl. Protein was pooled and concentrated using an Amicon 30K concentrator and incubated overnight on ice with the addition of TEV protease. Size-exclusion chromatography (SEC) was performed using a Superdex™ 200 10/300 GL increase (GE) column equilibrated in SEC buffer (20 mM HEPES pH 7.5, 150 mM NaCl and 0.5 mM TCEP). Fractions containing the protein of interest were pooled, concentrated, spun down to remove potential aggregate, and flash frozen in liquid nitrogen for storage at −80°C. c10orf76-PI4KB complex SEC trace was generated by mixing c10orf76 and PI4KB in a 1:1 ratio after individual anion exchange runs and then injecting onto the Superdex™ 200 10/300 GL increase (GE) column. Elution volumes of protein standards were obtained from the GE Instruction 29027271 AH size-exclusion chromatography columns document. See Protein kinase A (PKA) treatment of PI4KB for details on producing the phosphorylated variant of PI4KB.

ACBD3, Rab11a, and PKA

ACBD3 and Rab11a were expressed with N-terminal GST tags, with protein kinase A (*M. musculus* PKA catalytic subunit alpha; Addgene 14921) expressed with an N-terminal His tag. ACBD3, Rab11a, and PKA were expressed in BL21 C-41(DE3) *E. coli* cells, with ACBD3 and Rab11 expression carried out overnight at 16°C with 0.1 mM IPTG, and PKA expression was carried out for 4 h at 28°C with 1 mM IPTG. ACBD3, Rab11, and PKA were purified as previously published [11,14,59]. In brief, cell pellets containing expressed ACBD3 or Rab11a were sonicated in Q Buffer (20 mM Tris–HCl pH 8.0, 100 mM NaCl, 5% (v/v) glycerol, 2 mM β-mercaptoethanol) containing protease inhibitors (Millipore Protease Inhibitor Cocktail Set III, Animal-Free) for 5 min on ice. Triton X-100 (0.1% v/v) was added to the cell lysate, and the lysed cell solution was centrifuged for 45 min at 20,000 *g* at 2°C. Supernatant was filtered through a 5 μm filter and incubated with 1–4 ml of Glutathione Sepharose™ 4B beads (GE) for 1–2 h at 4°C. Beads were then washed with Q buffer, and GST-tagged proteins were eluted with 20 mM glutathione in Q buffer. Protein was further purified using anion exchange and size-exclusion chromatography as described above, and final protein was spun down to remove potential aggregate and flash frozen in liquid nitrogen for storage at −80°C. Nickel purification of PKA proceeded as described for PI4KB, and nickel elute was concentrated, spun down to remove potential aggregate, and flash frozen in liquid nitrogen for storage at −80°C.

Nickel and GST-Pulldown assays

For His pulldowns, NiNTA-agarose beads (Qiagen) (20 μl) were washed three times by centrifugation and resuspension in NiNTA buffer. His-tagged bait protein was then added to a concentration of 1–3 μM and incubated with the beads on ice for 10 min in a total volume of 50 μl. Beads were washed three times with 150 μl NiNTA buffer at 4°C. Non-His-tagged prey protein was then added to a final concentration of 1–2 μM in a total volume of 50 μl, at which point 10 μl was taken for SDS–PAGE analysis. The mixture was incubated on ice for an additional 30 min and then washed four times with 120 μl NiNTA buffer at 4°C at which time an aliquot was taken as the output for SDS–PAGE analysis.

For GST pulldowns, Glutathione Sepharose™ 4B beads (GE healthcare) were washed three times by centrifugation and resuspension in Q buffer. GST-tagged bait protein (or control GST) was then added to a concentration of 3–6 μM in 50 μl and incubated with the beads on ice for 10 min in a total volume of 50 μl. Beads were washed three times with 150 μl Q buffer at 4°C. Non-GST-tagged prey protein were then added to a final concentration of 2–4 μM in a total volume of 50 μl, at which point the input was taken for SDS–PAGE analysis.

The mixture was incubated on ice for an additional 30 min and then washed four times with 120 μl Q buffer at 4°C, at which time an aliquot was taken as the output for SDS–PAGE analysis.

Vesicle preparation and lipid kinase assays

Lipid kinase assays were carried out using the Transcreener® ADP^{2}FI Assay (BellBrook Labs) following the published protocol as previously described [11]. In brief, substrate stocks were made up containing 1.0 mg/ml PI vesicles or 4.0 mg/ml Golgi-mimetic vesicles (10% PS, 20% PI, 25% PE, 45% PC) and were extruded through a 100 nm Nanosizer Extruder (T&T Scientific) and then combined with in a buffer containing 20 mM HEPES pH 7.5, 100 mM KCl, and 0.5 mM EDTA (200 μM ATP with 1.0 mg/ml PI vesicles, 20 μM ATP with 1.0 mg/ml Golgi-mimetic vesicles). Kinase reactions were started by adding 2 μl of this substrate stock in a 384-well black low volume plates (Corning 4514). Proteins were thawed on ice and spun down to remove precipitate. Proteins were diluted individually to 4× the desired concentration in Kinase Buffer (40 mM HEPES pH 7.5, 200 mM NaCl, 20 mM MgCl$_2$, 0.8% Triton X-100, and 0.2 mM TCEP) on ice. Proteins were then mixed together or with additional Kinase buffer resulting in 2 × desired concentrations of each protein. To start the reaction, 2 μl of 2 × protein stock was added to 2 μl of 2 × substrate stock in plates. After mixing, the 4 μl reactions consisted of 30 mM HEPES pH 7.5 (RT), 100 mM NaCl, 50 mM KCl, 10 mM MgCl$_2$, 0.25 mM EDTA, 0.4% (v/v) Triton X-100, 0.1 mM TCEP, 10 μM ATP, and 0.5 mg/ml vesicles. PI4KB was run at a final concentration of 15, 20, or 40 nM, and c10orf76 was run in 4-fold curves from 1 μM to 3.9 nM, or 1.5 μM to 23 nM, or 5-fold curves from 2 μM to 1.6 nM. Reactions proceeded at 23°C for 20–30 min. Reactions were stopped using 4 μl of the transcreener stop buffer (1 × Stop & Detect Buffer B, 8 nM ADP Alexa594 Tracer, 97 μg/ml ADP2 Antibody-IRDye® QC-1). Fluorescence intensity was measured using a Spectramax M5 plate reader with λex x = 590 nm and λem m = 620 nm (20 nm bandwidth). Data were plotted using Graphpad Prism software, with IC$_{50}$ values determined by nonlinear regression (curve fit). No detectable nonspecific ATPase activity was detected in reactions containing 250 nM wild-type PI4KB without vesicle substrate.

Mapping the c10orf76-PI4KB binding interface using HDX-MS

Hydrogen–deuterium exchange reactions were conducted in 50 μl reactions with a final concentration of 400 nM of protein per sample (c10orf76-PI4KB, 400 nM each). Reactions were initiated by the addition of 45 μl of D$_2$O Buffer Solution (10 mM HEPES pH 7.5, 50 mM NaCl, 97% D$_2$O) to 5 μl of protein solution, to give a final concentration of 87% D$_2$O. Exchange was carried out for four timepoints (3 s at 1°C and 3 s, 30 s, and 300 s at 23°C). Exchange was terminated by the addition of acidic quench buffer giving a final concentration 0.6 M guanidine–HCl and 0.8% formic acid. All experiments were carried out in triplicate. Samples were immediately frozen in liquid nitrogen and stored at −80°C until mass analysis.

Comparison of FLH409AAA and WT c10orf76 secondary structure

Hydrogen–deuterium exchange mass spectrometry reactions were performed with 40 μl final volume with a protein concentration of

0.25 μM in each sample. Reactions were started by the addition of 39 μl D$_2$O buffer (100 mM NaCl, 35 mM HEPES, 91.7% D$_2$O) to 1 μl of protein (Final: 89.4% D$_2$O). Reactions were quenched by the addition of 30 μl of acidic quench buffer (3% formic acid, 2 M guanidine) resulting in final 1.28% Formic acid and 0.85 M guanidine–HCl. Proteins were allowed to undergo exchange reactions for either 3 s or 300 s at 23°C prior to addition of quench buffer and flash freezing in liquid N$_2$. All samples were set and run in triplicate. Samples were stored at −80°C until injection onto the UPLC for MS analysis.

HDX-MS data analysis

Protein samples were rapidly thawed and injected onto a UPLC system kept in a cold box at 2°C. The protein was run over two immobilized pepsin columns (Applied Biosystems; porosyme, 2-3131-00) stored at 10°C and 2°C at 200 μl/min for 3 min, and the peptides were collected onto a VanGuard precolumn trap (Waters). The trap was subsequently eluted in line with an Acquity 1.7 μm particle, 100 × 1 mm^2 C18 UPLC column (Waters), using a gradient of 5–36% B (buffer A 0.1% formic acid, buffer B 100% acetonitrile) over 16 min. MS experiments were performed on an Impact QTOF (Bruker), and peptide identification was done by running tandem MS (MS/MS) experiments run in data-dependent acquisition mode. The resulting MS/MS datasets were analyzed using PEAKS7 (PEAKS), and a false discovery rate was set at 1% using a database of purified proteins and known contaminants. HD-Examiner Software (Sierra Analytics) was used to automatically calculate the level of deuterium incorporation into each peptide. All peptides were manually inspected for correct charge state and presence of overlapping peptides. Deuteration levels were calculated using the centroid of the experimental isotope clusters. Attempts at generating fully deuterated protein samples to allow for the control of peptide back exchange levels during digestion and separation were made for all proteins. Protein was incubated with 3 M guanidine for 30 min prior to the addition of D$_2$O, where they were further incubated for an hour on ice. The reactions were then quenched as before. Generation of a fully deuterated sample was successful for PI4K using this method, however generation of fully deuterated c10orf76 failed. Results for c10orf76 are therefore presented as relative levels of deuterium incorporation, and the only control for back exchange was the level of deuterium present in the buffer (87%). The average error of all time points and conditions for each HDX project was < 0.2 Da. Therefore, changes in any peptide at any time point greater than both 7% and 0.5 Da between conditions with an unpaired *t*-test value of $P < 0.05$ were considered significant. The full details of H/D exchange for all peptides are shown in Source data, with statistics described in Table EV1. All HDX-MS data was analyzed according to the guidelines set out by the IC-HDX-MS community [60].

Protein kinase A (PKA) treatment of PI4KB

Protein kinase A (mouse catalytic subunit) was serially diluted, and different concentrations were incubated with PI4KB in 20 μl reactions on ice for 1 h (20 μg PI4KB, 20 mM MgCl$_2$, 200 μM ATP and either 840, 168, 34, 7, or 0 ng PKA). Reactions were terminated by the addition of acidic quench buffer giving a final concentration

0.6 M guanidine–HCl and 0.8% formic acid and then flash frozen in liquid N_2 prior to MS phosphorylation analysis.

To generate *E. coli* expressed, PKA phosphorylated PI4KB for use in kinase assays and HDX-MS, phosphorylation of Ser496 was carried out using 1.0 mg PI4KB, 20 mM $MgCl_2$, 200 μM ATP, and 4.2 μg PKA in NiNTA buffer, with the reaction allowed to proceed for 1 h on ice. The reaction was quenched with 20 mM EDTA and immediately loaded onto a GE 1 ml HisTap FF crude to remove His-tagged PKA. Phosphorylated PI4KB was concentrated followed by size-exclusion chromatography as described for PI4KB above. In tandem, a non-phosphorylated PI4KB control was purified in the same manner except $MgCl_2$, ATP, and PKA were not added. Protein was flash-frozen in liquid N_2 for storage at −80°C.

HDX-MS dose response of c10orf76 of phosphorylated PI4KB

Phosphorylated and non-phosphorylated PI4KB were generated and purified as described above. HDX reactions were conducted in 130 μl reaction volumes with a final concentration of 20 nM PI4KB (phosphorylated or non-phosphorylated) per sample, with 0, 5, 10, 20, 40, 80, 160, and 320 nM c10orf76. Exchange was carried out for 5 s, in triplicate for each concentration of c10orf76. Hydrogen–deuterium exchange was initiated by the addition of 80 μl of D_2O buffer solution (10 mM HEPES (pH 7.5), 50 mM NaCl, 97% D_2O) to the protein solution, to give a final concentration of 60% D_2O. Exchange was terminated by the addition of 20 μl ice-cold acidic quench buffer at a final concentration 0.6 M guanidine–HCl and 0.9% formic acid. Samples were immediately frozen in liquid nitrogen at −80°C. Data analyzed as described above in HDX-MS data analysis.

Phosphorylation analysis

LC-MS/MS analysis of phosphorylated variants of PI4KB was carried out as described in the HDX-MS data analysis section. MS/MS datasets were analyzed using PEAKS7 to identify phosphorylated peptides in PI4KB and c10orf76. A false discovery rate was set at 0.1% using a database of purified proteins and known contaminants. To measure PI4KB phosphorylation levels using Bruker Data analysis, the phosphorylated and non-phosphorylated peptides of interest were extracted, and the total area of each peptide was manually integrated to determine the amount of phosphorylated vs non-phosphorylated species under given experimental conditions. No phosphorylation was detected in *E. coli* derived PI4KB. For *Sf9*-derived PI4KB Ser294 phosphorylation, the peptides KRTAS* NPKVENEDE (290–303) and KRTAS*NPKVENEDEPVRLADERE (290–312) were averaged; for Ser413 phosphorylation, DTTSVPARI-PENRIRSTRS*VENLPECGITHE (395–425) was used; for Ser430 phosphorylation, GITHEQRAGS*F (430–441) was used; and for Ser496 phosphorylation, IAAGDIRRRLS*EQLAHTPTA (486–505) and IAAGDIRRRLS*EQ-LAHTPTAF (486–506) were averaged. No phosphorylation was detected in *E. coli*-derived c10orf76. For *Sf9*-derived c10orf76 Ser14 phosphorylation, LRKSS*ASKKPLKE (10–22) was used, and for the 325–351 phosphorylation (exact location of phosphorylation ambiguous), VTTPVSPAPTTPVTPLGTTPPSSD (326–348), VTTPVSPAPTTPVTPLGTTPPSSDVISS (325–351), and VT TPVSPAPTTPVTPLGTTPPSS (325–347) were averaged.

Isothermal titration calorimetry

Purified c10orf76, non-phosphorylated PI4KB, and Ser496-phosphorylated PI4KB were dialyzed separately into buffer containing 20 mM HEPES pH 7.5, 150 mM NaCl, and 0.5 mM TCEP. All ITC experiments were carried out at 20°C on a MicroCal iTC200 instrument (GE Healthcare). The sample cell contained non-phosphorylated PI4KB or Ser496-phosphorylated PI4KB (5 μM), and c10orf76 (50 μM) was added in 19 injections of 2 μl each. Data were processed using Origin software (MicroCal) and the dissociation constants (Kd) were determined using a one-site model. Figures are of a single experiment, but are representative of three independent experiments using protein from two different protein preparations.

Alignments

Protein sequences from the Uniprot database were aligned using Clustal Omega [61], and figures were generated using ESPript [62]. Uniprot PI4KB entries used: *H. sapiens* (Q9UBF8-2), *M. musculus* (Q8BKC8), *D. rerio* (Q49GP3), *D. melanogaster* (Q9BKJ2), *C. elegans* (Q20077). Uniprot c10orf76 entries used: *H. sapiens* (Q5T2E6), *M. musculus* (Q6PD19), *D. rerio* (Q6PGW3), *D. melanogaster* (Q7KSU3).

DNA constructs and antibodies

The following antibodies were used to examine protein localization in WT and c10orf76 knockout HAP1 cells. Mouse monoclonal antibodies included anti-GBF1 (BD Biosciences), anti-CM1 (a gift from Felix Wieland, Heidelberg University, Germany), anti-GM130 (BD Biosciences), anti-Giantin (Enzo Life Science), anti-ERGIC53 (Enzo Life Science), anti-βCOP (Sigma), anti-PI4P (Echelon), and anti-ACBD3 (Sigma). Rabbit polyclonal antibodies included anti-PI4KB (Millipore), anti-COPI α/γ (a gift from Felix Wieland), and anti-TGN46 (Novus Biologicals). Conjugated goat anti-rabbit and goat anti-mouse Alexa Fluor 488, 596, or 647 (Molecular Probes) were used as secondary antibodies.

The following antibodies were used for Western blot analysis to examine protein expression level in WT and c10orf76 knockout HAP1 cells. Mouse monoclonal antibodies included anti-GBF1 (BD Biosciences), anti-β-actin (Sigma), and Rabbit polyclonal antibodies included anti-PI4KB (Millipore). IRDye-conjugated goat anti-mouse or anti-rabbit (LI-COR) were used as secondary antibodies.

GFP-PI4KB, GFP-PI4KB RL494EA, GFP-c10orf76, and GFP-c10orf76 FLH409AAA were cloned using Gibson assembly [63] into the pEGFP-C1 vector (Clonetech). mRFP-FKBP12-PI4KB and mRFP-FKBP12-PI4KB RL494EA were generated by amplifying the mRFP-FKBP12 insert from mRFP-FKBP12-5ptpase domain [64] and replacing the N-terminal GFP in either GFP-PI4KB or GFP-PI4KB RL494EA using a single digest with NdeI. AKAP-FRB-CFP, which is used to selectively recruit FKBP12-tagged proteins to the outer mitochondrial membrane, has been described previously [65].

Cell culture, transfection, and live-cell confocal microscopy of rapamycin recruitment

HEK293-AT1 cells, which stably express the AT1a rat Angiotensin II receptor [66], were cultured in Dulbecco's modified Eagle medium

(DMEM-high glucose) containing 10% (vol/vol) FBS and supplemented with a 1% solution of penicillin/streptomycin. This cell line is regularly tested for *Mycoplasma* contamination using a commercially available detection kit (InvivoGen) and, after thawing, the cells are treated with plasmocin prophylactic (InvivoGen) at 500 μg/ml for the initial three passages (6–9 days) as well as supplemented with 5 μg/ml of plasmocin prophylactic for all subsequent passages.

For confocal microscopy, HEK293-AT1 cells (3×10^5 cells/well) were plated on 29-mm circular glass-bottom culture dishes (#1.5; Cellvis) pre-coated with 0.01% poly-L-lysine solution (Sigma). The cells were allowed to attach overnight prior to transfection of plasmid DNAs (0.1–0.2 μg/well) using Lipofectamine 2000 (Invitrogen) and Opti-MEM (Invitrogen) according to the manufacturer's instructions. Please note that studies using the rapamycin-inducible protein heterodimerization system used a 1:2:1 ratio of plasmid DNA for transfection of the FKBP12-tagged PI4KB enzyme, AKAP-FRB-CFP recruiter, and GFP-c10orf76 variant (total DNA: 0.4 μg/well). After 18–20 h of transfection, cells were incubated in 1 ml of modified Krebs-Ringer solution (containing 120 mM NaCl, 4.7 mM KCl, 2 mM $CaCl_2$, 0.7 mM $MgSO_4$, 10 mM glucose, 10 mM HEPES, and adjusted to pH 7.4) and images were acquired at room temperature using a Zeiss LSM 710 laser-scanning confocal microscope (Carl Zeiss Microscopy). Rapamycin treatment of cells was carried out at a final concentration of 100 nM. Image acquisition was performed using the ZEN software system (Carl Zeiss Microscopy), while the image preparation was done using the open-source FIJI platform [67].

Cell culture, transfection, and live-cell confocal microscopy of HAP1 WT and c10orf76 knockout cells

Cells and viruses

HAP1 WT cells and HAP1 c10orf76 knockout cells were obtained from T. Brummelkamp, and are now carried by Horizon Discovery. The generation and validation of the Hap1 c10orf76 KO cell clone was described previously [28]. HeLa R19 cells were obtained from G. Belov (University of Maryland and Virginia-Maryland Regional College of Veterinary Medicine, US). HeLa PI4KB knockout cells were described previously [29]. HAP1 cells were cultured in IMDM (Thermo Fisher Scientific) supplemented with 10% fetal calf serum (FCS) and penicillin–streptomycin. HeLa cells were cultured in DMEM (Lonza) supplemented with 10% FCS and penicillin–streptomycin. All cells were grown at 37°C in 5% CO_2. The following enteroviruses were used: CVA10 (strain Kowalik, obtained from the National Institute for Public Health and Environment; RIVM, The Netherlands), CVB3 (strain Nancy, obtained by transfection of the infectious clone p53CB3/T7 as described previously [68]), and PV1 (strain Sabin, ATCC). Virus titers were determined by end-point titration analysis and expressed as 50% tissue culture infectious dose ($TCID_{50}$).

Replication rescue assay

HeLa cells were transfected with plasmids carrying WT or mutant PI4KB (RL494EA), Golgi-targeting EGFP (pEGFP-GalT), or kinase-dead PI4KB (PI4KB-KD) as a negative control. At 24 h post-transfection, the cells were infected with CVA10, CVB3, and PV1. At 8 h p.i., the infected cells were frozen, and virus titers were determined by end-point titration analysis and expressed as 50% tissue culture infectious dose ($TCID_{50}$).

Immunofluorescence microscopy of WT and c10orf76 knockout HAP1 cells

HAP1 cells were grown on ibiTreat slides μ-slide 18-wells (Ibidi) one day prior to infection. Cells were fixed by submersion in a 4% paraformaldehyde solution for 15 min. Nuclei were stained with DAPI. Confocal imaging was performed with a Leica SpeII confocal microscope.

Expanded View for this article is available online.

Author contributions

JAM, RMH, MLJ, and JTBS expressed and purified proteins. JAM and JEB designed complex-disrupting mutations. JAM carried out pulldown and kinase assays. JAM, MLJ, RMH, and JEB carried out HDX-MS and analysis. CJP, JAM, and MJB performed ITC. HL and WE performed viral infection assays, and HL characterized c10orf76 knockout cells. JGP and TB performed cellular c10orf76 recruitment experiments. JAM, JRPMS, TB, FJMK, and JEB designed the research. JAM and JEB wrote the manuscript with input from all authors.

Conflict of interest

The authors declare that they have no conflict of interest.

References

1. Tan J, Brill JA (2014) Cinderella story: PI4P goes from precursor to key signaling molecule. *Crit Rev Biochem Mol Biol* 49: 33–58

2. Balla T (2013) Phosphoinositides: tiny lipids with giant impact on cell regulation. *Physiol Rev* 93: 1019–1137

3. Weber SS, Ragaz C, Reus K, Nyfeler Y, Hilbi H (2006) Legionella pneumophila exploits PI(4)P to anchor secreted effector proteins to the replicative vacuole. *PLoS Pathog* 2: e46

4. Hsu N-Y, Ilnytska O, Belov G, Santiana M, Chen Y-H, Takvorian PM, Pau C, van der Schaar H, Kaushik-Basu N, Balla T *et al* (2010) Viral reorganization of the secretory pathway generates distinct organelles for RNA replication. *Cell* 141: 799–811

5. van der Schaar HM, Dorobantu CM, Albulescu L, Strating JRPM, van Kuppeveld FJM (2016) Fat(al) attraction: picornaviruses usurp lipid transfer at membrane contact sites to create replication organelles. *Trends Microbiol* 24: 535–546

6. Burke JE (2018) Structural basis for regulation of phosphoinositide kinases and their involvement in human disease. *Mol Cell* 71: 653−673

7. Dornan GL, McPhail JA, Burke JE (2016) Type III phosphatidylinositol 4 kinases: structure, function, regulation, signalling and involvement in disease. *Biochem Soc Trans* 44: 260−266

8. Boura E, Nencka R (2015) Phosphatidylinositol 4-kinases: function, structure, and inhibition. *Exp Cell Res* 337: 136−145

9. Mesmin B, Bigay J, Polidori J, Jamecna D, Lacas-Gervais S, Antonny B (2017) Sterol transfer, PI4P consumption, and control of membrane lipid order by endogenous OSBP. *EMBO J* 36: 3156−3174

10. Lu D, Sun H-Q, Wang H, Barylko B, Fukata Y, Fukata M, Albanesi JP, Yin HL (2012) Phosphatidylinositol 4-kinase IIα is palmitoylated by Golgi-localized palmitoyltransferases in cholesterol-dependent manner. *J Biol Chem* 287: 21856−21865

11. McPhail JA, Ottosen EH, Jenkins ML, Burke JE (2017) The molecular basis of aichi virus 3A protein activation of phosphatidylinositol 4 kinase IIIβ, PI4KB, through ACBD3. *Structure* 25: 121−131

12. Klima M, Tóth DJ, Hexnerova R, Baumlová A, Chalupská D, Tykvart J, Rezabkova L, Sengupta N, Man P, Dubankova A *et al* (2016) Structural insights and *in vitro* reconstitution of membrane targeting and activation of human PI4KB by the ACBD3 protein. *Sci Rep* 6: 23641

13. Sasaki J, Ishikawa K, Arita M, Taniguchi K (2012) ACBD3-mediated recruitment of PI4KB to picornavirus RNA replication sites. *EMBO J* 31: 754−766

14. Burke JE, Inglis AJ, Perisic O, Masson GR, McLaughlin SH, Rutaganira F, Shokat KM, Williams RL (2014) Structures of PI4KIIIβ complexes show simultaneous recruitment of Rab11 and its effectors. *Science* 344: 1035−1038

15. Altan-Bonnet N, Balla T (2012) Phosphatidylinositol 4-kinases: hostages harnessed to build panviral replication platforms. *Trends Biochem Sci* 37: 293−302

16. Téoulé F, Brisac C, Pelletier I, Vidalain P-O, Jégouic S, Mirabelli C, Bessaud M, Combelas N, Autret A, Tangy F *et al* (2013) The Golgi protein ACBD3, an interactor for poliovirus protein 3A, modulates poliovirus replication. *J Virol* 87: 11031−11046

17. Greninger AL, Knudsen GM, Betegon M, Burlingame AL, DeRisi JL (2013) ACBD3 interaction with TBC1 domain 22 protein is differentially affected by enteroviral and kobuviral 3A protein binding. *MBio* 4: e00098-13

18. Greninger AL, Knudsen GM, Betegon M, Burlingame AL, DeRisi JL (2012) The 3A protein from multiple picornaviruses utilizes the golgi adaptor protein ACBD3 to recruit PI4KIIIβ. *J Virol* 86: 3605−3616

19. Fowler ML, McPhail JA, Jenkins ML, Masson GR, Rutaganira FU, Shokat KM, Williams RL, Burke JE (2016) Using hydrogen deuterium exchange mass spectrometry to engineer optimized constructs for crystallization of protein complexes: case study of PI4KIIIβ with Rab11. *Protein Sci* 25: 826−839

20. de Graaf P, Zwart WT, van Dijken RAJ, Deneka M, Schulz TKF, Geijsen N, Coffer PJ, Gadella BM, Verkleij AJ, van der Sluijs P *et al* (2004) Phosphatidylinositol 4-kinasebeta is critical for functional association of rab11 with the Golgi complex. *Mol Biol Cell* 15: 2038−2047

21. Godi A, Pertile P, Meyers R, Marra P, Di Tullio G, Iurisci C, Luini A, Corda D, De Matteis MA (1999) ARF mediates recruitment of PtdIns-4-OH kinase-beta and stimulates synthesis of PtdIns(4,5)P2 on the Golgi complex. *Nat Cell Biol* 1: 280−287

22. Hausser A, Storz P, Märtens S, Link G, Toker A, Pfizenmaier K (2005) Protein kinase D regulates vesicular transport by phosphorylating and activating phosphatidylinositol-4 kinase IIIbeta at the Golgi complex. *Nat Cell Biol* 7: 880−886

23. Hausser A, Link G, Hoene M, Russo C, Selchow O, Pfizenmaier K (2006) Phospho-specific binding of 14-3-3 proteins to phosphatidylinositol 4-kinase III beta protects from dephosphorylation and stabilizes lipid kinase activity. *J Cell Sci* 119: 3613−3621

24. Chalupská D, Eisenreichova A, Rózycki B, Rezabkova L, Humpolickova J, Klima M, Boura E (2017) Structural analysis of phosphatidylinositol 4-kinase IIIβ (PI4KB) − 14-3-3 protein complex reveals internal flexibility and explains 14-3-3 mediated protection from degradation *in vitro*. *J Struct Biol* 200: 36−44

25. Isobe K, Jung HJ, Yang C-R, Claxton J, Sandoval P, Burg MB, Raghuram V, Knepper MA (2017) Systems-level identification of PKA-dependent signaling in epithelial cells. *Proc Natl Acad Sci USA* 114: E8875−E8884

26. Szivak I, Lamb N, Heilmeyer LMG (2006) Subcellular localization and structural function of endogenous phosphorylated phosphatidylinositol 4-kinase (PI4K92). *J Biol Chem* 281: 16740−16749

27. Jovic M, Kean MJ, Szentpetery Z, Polevoy G, Gingras A-C, Brill JA, Balla T (2012) Two phosphatidylinositol 4-kinases control lysosomal delivery of the Gaucher disease enzyme, β-glucocerebrosidase. *Mol Biol Cell* 23: 1533−1545

28. Blomen VA, Májek P, Jae LT, Bigenzahn JW, Nieuwenhuis J, Staring J, Sacco R, van Diemen FR, Olk N, Stukalov A *et al* (2015) Gene essentiality and synthetic lethality in haploid human cells. *Science* 350: 1092−1096

29. Lyoo H, van der Schaar HM, Dorobantu CM, Rabouw HH, Strating JRPM, van Kuppeveld FJM (2019) ACBD3 is an essential pan-enterovirus host factor that mediates the interaction between viral 3A protein and cellular protein PI4KB. *MBio* 10: 282

30. Xiao X, Lei X, Zhang Z, Ma Y, Qi J, Wu C, Xiao Y, Li L, He B, Wang J (2017) Enterovirus 3A facilitates viral replication by promoting PI4KB-ACBD3 interaction. *J Virol* 91: 799

31. Klima M, Chalupská D, Rózycki B, Humpolickova J, Rezabkova L, Silhan J, Baumlová A, Dubankova A, Boura E (2017) Kobuviral non-structural 3A proteins act as molecular harnesses to hijack the host ACBD3 protein. *Structure* 25: 219−230

32. Ishikawa-Sasaki K, Sasaki J, Taniguchi K (2014) A complex comprising phosphatidylinositol 4-kinase IIIβ, ACBD3, and Aichi virus proteins enhances phosphatidylinositol 4-phosphate synthesis and is critical for formation of the viral replication complex. *J Virol* 88: 6586−6598

33. Wessels E, Duijsings D, Niu T-K, Neumann S, Oorschot VM, de Lange F, Lanke KHW, Klumperman J, Henke A, Jackson CL *et al* (2006) A viral protein that blocks Arf1-mediated COP-I assembly by inhibiting the guanine nucleotide exchange factor GBF1. *Dev Cell* 11: 191−201

34. Lanke KHW, van der Schaar HM, Belov GA, Feng Q, Duijsings D, Jackson CL, Ehrenfeld E, van Kuppeveld FJM (2009) GBF1, a guanine nucleotide exchange factor for Arf, is crucial for coxsackievirus B3 RNA replication. *J Virol* 83: 11940−11949

35. Wessels E, Duijsings D, Lanke KHW, van Dooren SHJ, Jackson CL, Melchers WJG, van Kuppeveld FJM (2006) Effects of picornavirus 3A Proteins on Protein Transport and GBF1-dependent COP-I recruitment. *J Virol* 80: 11852−11860

36. Ilnytska O, Santiana M, Hsu N-Y, Du W-L, Chen Y-H, Viktorova EG, Belov G, Brinker A, Storch J, Moore C *et al* (2013) Enteroviruses harness the cellular endocytic machinery to remodel the host cell cholesterol landscape for effective viral replication. *Cell Host Microbe* 14: 281−293

37. Masson GR, Jenkins ML, Burke JE (2017) An overview of hydrogen deuterium exchange mass spectrometry (HDX-MS) in drug discovery. *Expert Opin Drug Discov* 12: 981−994

38. Vadas O, Jenkins ML, Dornan GL, Burke JE (2017) Using hydrogen-deuterium exchange mass spectrometry to examine protein-membrane interactions. *Meth Enzymol* 583: 143–172

39. Vadas O, Burke JE (2015) Probing the dynamic regulation of peripheral membrane proteins using hydrogen deuterium exchange-MS (HDX-MS). *Biochem Soc Trans* 43: 773–786

40. Hornbeck PV, Zhang B, Murray B, Kornhauser JM, Latham V, Skrzypek E (2015) PhosphoSitePlus, 2014: mutations, PTMs and recalibrations. *Nucleic Acids Res* 43: D512–D520

41. Ward DG, Ashton PR, Trayer HR, Trayer IP (2001) Additional PKA phosphorylation sites in human cardiac troponin I. *Eur J Biochem* 268: 179–185

42. Marx SO, Reiken S, Hisamatsu Y, Jayaraman T, Burkhoff D, Rosemblit N, Marks AR (2000) PKA phosphorylation dissociates FKBP12.6 from the calcium release channel (ryanodine receptor): defective regulation in failing hearts. *Cell* 101: 365–376

43. Zhu MM, Rempel DL, Du Z, Gross ML (2003) Quantification of protein-ligand interactions by mass spectrometry, titration, and H/D exchange: PLIMSTEX. *J Am Chem Soc* 125: 5252–5253

44. Hammond GRV, Fischer MJ, Anderson KE, Holdich J, Koteci A, Balla T, Irvine RF (2012) PI4P and PI(4,5)P2 are essential but independent lipid determinants of membrane identity. *Science* 337: 727–730

45. van der Schaar HM, van der Linden L, Lanke KHW, Strating JRPM, Pürstinger G, de Vries E, de Haan CAM, Neyts J, van Kuppeveld FJM (2012) Coxsackievirus mutants that can bypass host factor PI4KIIIβ and the need for high levels of PI4P lipids for replication. *Cell Res* 22: 1576–1592

46. Palmer DJ, Helms JB, Beckers CJ, Orci L, Rothman JE (1993) Binding of coatomer to Golgi membranes requires ADP-ribosylation factor. *J Biol Chem* 268: 12083–12089

47. Staring J, von Castelmur E, Blomen VA, van den Hengel LG, Brockmann M, Baggen J, Thibaut HJ, Nieuwenhuis J, Janssen H, van Kuppeveld FJM *et al* (2017) PLA2G16 represents a switch between entry and clearance of Picornaviridae. *Nature* 541: 412–416

48. Flanagan CA, Schnieders EA, Emerick AW, Kunisawa R, Admon A, Thorner J (1993) Phosphatidylinositol 4-kinase – gene structure and requirement for yeast-cell viability. *Science* 262: 1444–1448

49. Walch-Solimena C, Novick P (1999) The yeast phosphatidylinositol-4-OH kinase pik1 regulates secretion at the Golgi. *Nat Cell Biol* 1: 523–525

50. Nakanishi S, Catt KJ, Balla T (1995) A wortmannin-sensitive phosphatidylinositol 4-kinase that regulates hormone-sensitive pools of inositolphospholipids. *Proc Natl Acad Sci USA* 92: 5317–5321

51. Balla T, Downing GJ, Jaffe H, Kim S, Zolyomi A, Catt KJ (1997) Isolation and molecular cloning of wortmannin-sensitive bovine type III phosphatidylinositol 4-kinases. *J Biol Chem* 272: 18358–18366

52. Meyers R, Cantley LC (1997) Cloning and characterization of a wortmannin-sensitive human phosphatidylinositol 4-kinase. *J Biol Chem* 272: 4384–4390

53. Sohda M, Misumi Y, Yamamoto A, Yano A, Nakamura N, Ikehara Y (2001) Identification and characterization of a novel Golgi protein, GCP60, that interacts with the integral membrane protein giantin. *J Biol Chem* 276: 45298–45306

54. Polevoy G, Wei H-C, Wong R, Szentpetery Z, Kim YJ, Goldbach P, Steinbach SK, Balla T, Brill JA (2009) Dual roles for the *Drosophila* PI 4-kinase four wheel drive in localizing Rab11 during cytokinesis. *J Cell Biol* 187: 847–858

55. Dickinson ME, Flenniken AM, Ji X, Teboul L, Wong MD, White JK, Meehan TF, Weninger WJ, Westerberg H, Adissu H *et al* (2016) High-throughput discovery of novel developmental phenotypes. *Nature* 537: 508–514

56. Wang Y, Mousley CJ, Lete MG, Bankaitis VA (2019) An equal opportunity collaboration between lipid metabolism and proteins in the control of membrane trafficking in the trans-Golgi and endosomal systems. *Curr Opin Cell Biol* 59: 58–72

57. Viktorova EG, Gabaglio S, Meissner JM, Lee E, Moghimi S, Sztul E, Belov GA (2019) A redundant mechanism of recruitment underlies the remarkable plasticity of the requirement of poliovirus replication for the cellular ArfGEF GBF1. *J Virol* 93: e00856-19.

58. Spickler C, Lippens J, Laberge M-K, Desmeules S, Bellavance É, Garneau M, Guo T, Hucke O, Leyssen P, Neyts J *et al* (2013) Phosphatidylinositol 4-kinase III beta is essential for replication of human rhinovirus and its inhibition causes a lethal phenotype *in vivo*. *Antimicrob Agents Chemother* 57: 3358–3368

59. Slice LW, Taylor SS (1989) Expression of the catalytic subunit of cAMP-dependent protein kinase in Escherichia coli. *J Biol Chem* 264: 20940–20946

60. Masson GR, Burke JE, Ahn NG, Anand GS, Borchers C, Brier S, Bou-Assaf GM, Engen JR, Englander SW, Faber J *et al* (2019) Recommendations for performing, interpreting and reporting hydrogen deuterium exchange mass spectrometry (HDX-MS) experiments. *Nat Methods* 16: 595–602

61. Sievers F, Wilm A, Dineen D, Gibson TJ, Karplus K, Li W, Lopez R, McWilliam H, Remmert M, Söding J *et al* (2011) Fast, scalable generation of high-quality protein multiple sequence alignments using Clustal Omega. *Mol Syst Biol* 7: 539

62. Robert X, Gouet P (2014) Deciphering key features in protein structures with the new ENDscript server. *Nucleic Acids Res* 42: W320–W324

63. Gibson DG, Young L, Chuang R-Y, Venter JC, Hutchison CA, Smith HO (2009) Enzymatic assembly of DNA molecules up to several hundred kilobases. *Nat Methods* 6: 343–345

64. Várnai P, Thyagarajan B, Rohacs T, Balla T (2006) Rapidly inducible changes in phosphatidylinositol 4,5-bisphosphate levels influence multiple regulatory functions of the lipid in intact living cells. *J Cell Biol* 175: 377–382

65. Csordás G, Várnai P, Golenár T, Roy S, Purkins G, Schneider TG, Balla T, Hajnóczky G (2010) Imaging interorganelle contacts and local calcium dynamics at the ER-mitochondrial interface. *Mol Cell* 39: 121–132

66. Hunyady L, Baukal AJ, Gaborik Z, Olivares-Reyes JA, Bor M, Szaszak M, Lodge R, Catt KJ, Balla T (2002) Differential PI 3-kinase dependence of early and late phases of recycling of the internalized AT1 angiotensin receptor. *J Cell Biol* 157: 1211–1222

67. Schindelin J, Arganda-Carreras I, Frise E, Kaynig V, Longair M, Pietzsch T, Preibisch S, Rueden C, Saalfeld S, Schmid B *et al* (2012) Fiji: an open-source platform for biological-image analysis. *Nat Methods* 9: 676–682

68. Wessels E, Duijsings D, Notebaart RA, Melchers WJG, van Kuppeveld FJM (2005) A proline-rich region in the coxsackievirus 3A protein is required for the protein to inhibit endoplasmic reticulum-to-golgi transport. *J Virol* 79: 5163–5173